Modelling the terrestrial nitrogen and phosphorus cycle in the UVic ESCM

Makcim De Sisto [1,2], Andrew H. MacDougall [1], Nadine Mengis [3], and Sophia Antoniello [1]

[1]St. Francis Xavier University, Antigonish, NS, Canada
[2]Faculty of Engineering and Applied Science, Memorial University of Newfoundland, NL, Canada
[3]GEOMAR Helmholtz Centre for Ocean Research Kiel, Kiel, Germany

Correspondence: Makcim De Sisto (mdesisto@stfx.ca)

Abstract. Nitrogen (N) and ~~phosphorus~~ Phosphorus (P) biogeochemical dynamics are crucial for the regulation of the terrestrial carbon cycle. In Earth System Models (ESMs) the implementation of nutrient limitations has been shown to improve the carbon cycle feedback representation and hence, improve the fidelity of the response of land to simulated atmospheric CO_2 rise. Here we aimed to implement a terrestrial ~~nitrogen and phosphorus~~ N and P cycle in an Earth system model of intermediate complexity to improve projections of the future CO_2 fertilization feedbacks. The ~~nitrogen~~ N cycle is an improved version of the Wania et al. (2012) ~~nitrogen~~ N module, with enforcement of N mass conservation and the merger with a deep land-surface and wetland module that allows for the estimation of N_2O and NO fluxes. The N cycle module estimates fluxes from three organic (litter, soil organic matter and vegetation) and two inorganic (NH_4^+ ~~+and~~ NO_3^-) pools, accounts for inputs from biological ~~nitrogen~~ N fixation and N deposition. The P cycle module contains the same organic pools with one inorganic P pool, it estimates influx of P from rock weathering and losses from leaching and occlusion. Two historical simulations are carried for the different nutrient limitation setups of the model: ~~carbon and nitrogen~~ Carbon and Nitrogen (CN) and ~~carbon, nitrogen and phosphorus~~ Carbon, Nitrogen and Phosphorus (CNP), with a baseline carbon only simulation. The improved N cycle module now conserves mass and the added fluxes (NO and N_2O), along with the N and P pools are within the range of other studies and literature. For the years ~~2010-2020~~ 2001-2015 the nutrient limitation resulted in a reduction of GPP from the ~~Carbon-Nitrogen model version of 133~~ Carbon-only value of 143 PgC yr^{-1} ~~and the Carbon-Nitrogen-Phosphorus model version of 129~~ to 130 PgC yr^{-1} ~~simulations compared to Carbon only value of 143~~ in the CN version and 127 PgC yr^{-1} in the CNP version. This implies that the model efficiently represents a nutrient limitation over the CO_2 fertilization effect. CNP simulation resulted in a reduction of ~~10~~11% of the mean GPP and a reduction of 23% of the vegetation biomass compared to baseline C simulation. These results are in better agreement with observations, particularly in tropical regions where P limitation is known to be important. In summary, the implementation of the ~~nitrogen and phosphorus~~ N and P cycle have successfully enforced a nutrient limitation in the terrestrial system, which now have reduced the primary productivity and the capacity of land to uptake atmospheric carbon better matching observations.

1 Introduction

Terrestrial biogeochemical cycles are sensitive to changes in atmospheric CO_2 concentrations and climate. Their global evolution will determine the capacity of vegetation and soils to store anthropogenic carbon (Goll et al. , 2012). In terrestrial ecosystems carbon cycle feedbacks are constrained in part by the availability of nutrients (Fisher et al. , 2012; Zaehle et al. , 2014; Wieder et al. , 2015; Du et al. , 2020). Among nutrients ~~nitrogen and phosphorus~~ Nitrogen (N) and Phosphorus (P) are considered to be the most critical for limiting the primary productivity (Filipelli , 2002; Fowler et al. , 2013). Both are fundamental functional needs for plant biochemistry and their requirement is common in all vegetation taxa (Filipelli , 2002; Vitousek et al. , 2010; Du et al. , 2020). Regionally, the availability of nutrients can impair the photosynthetic efficiency of terrestrial vegetation and consequently their response to increasing atmospheric CO_2. Hence, in Earth System Models (ESMs) the representation of nutrient limitations is an imperative to improve the accuracy of carbon feedback projections and estimation of carbon budgets.

The simulations from first generation ESMs with carbon only schemes, have very likely overestimated the response of the terrestrial ecosystem to the increase of atmospheric CO_2 concentrations (Hungate et al. , 2003; Thorton et al. , 2007), showing a high terrestrial carbon uptake response which would require an unrealistic large nutrient supply. The addition of a ~~nitrogen~~ N cycle to the land system in ESMs has shown an overall reduction in the effect of CO_2 fertilization especially in high latitudes, with a weaker response in low latitudes which are typically P limited in natural systems (Wang et al. , 2007, 2010; Goll et al. , 2017; Du et al. , 2020; Wang et al. , 2020).

The global distribution of N and P is dependent on the biogeochemical characteristics of each nutrient. N inputs are mainly from Biological Nitrogen Fixation (BNF) and atmospheric deposition with little addition from rock weathering (Du et al. , 2020). There are two types of ~~nitrogen~~ N deposition from the atmosphere: wet (precipitation) and dry (particles). Among the two, wet deposition represents most of the atmospheric ~~nitrogen~~ N input (Fowler et al. , 2013; Dynarski et al. , 2019). In contrast, the main input of P comes from rock weathering (mainly apatite) with lesser inputs from atmospheric deposition as dust particles. These characteristic are among the reasons of a global spatial pattern where young soils are usually N limited and old soil are P limited (Filipelli , 2002; Fowler et al. , 2013; Du et al. , 2020). N accumulates rapidly from BNF where ~~nitrogen~~ N fixers are abundant and slowly where atmospheric deposition is dominant. Thereby, old soils have a larger accumulation of N especially in regions where ~~nitrogen~~ N fixers are abundant. On other hand, P input is limited by the parent material and the bioavailability is further constrain by the retention of recalcitrant P in soils. Walker and Syers (1976) even suggested that P storage has a fix total that cannot be rapidly replenished as parent material is limited.

These notions led to the common conceptualization that high latitudes are N limited while tropical regions are P limited. While this generalization is correct in most observational studies, the complex pattern of limitation is more intricate, and P limitation could be more common than is commonly inferred. Du et al. (2020) found that globally 43% of the terrestrial system are relatively limited by P while only 18% limited by N with the rest being co-limited by both. Biochemically, the availability of N and P can directly limit on another. The addition of P has been shown to be positive for the ~~nitrogen~~ N fixation, leading to the replenishment of N is ecosystems (Eisele et al. , 1989). N supply on the other hand regulates the production of the enzyme

phosphatase that cleaves ester-P bonds in soil organic matter (McGill and Cole , 1981; Olander and Vitousek , 2000; Wang et al. , 2007).

Biodiversity plays a crucial role in biogeochemical cycles. ~~Microbial diversity for exampleenables nitrogen pathways that only some taxa can metabolize.~~ The fluxes and availability of N and P in soils depends on the interactions between soil mineral matrix, plants and microbes (Cotrufo et al. , 2013). For example, N input from atmospheric N_2 fixation is mediated by a specialized group of microorganisms. Furthermore, the recycling on N from plants-soil-microbes determines the availability of N for plant uptake. Overall, the land biota dynamics impacts the productivity, ecosystem resiliense and stability (Yang et al. , 2018) . High diversity has been linked to enhanced vegetation productivity (Wagg et al. , 2014). The diversity in terrestrial ecosystem is determined by biological, environmental and physico-chemical processes. Anthropogenic activities can influence soil diversity, impacting the availability and cycling of N and P (Chen et al. , 2019). For example, N and P fertilization, have been shown to affect soil microbial biomass and composition (Ryan et al. , 2009). Plant diversity, is linked to soil health and functioning, and is core for the ~~nitrogen and phosphorus~~ N and P cycles. Vegetation species variable adaption to nutrient concentrations also plays a role in the availability of nutrients in soils and the biogeography of terrestrial vegetation. Overall, biodiversity constitute an environmental resilience factor to abrupt changes (Van Oijen et al. , 2020). However, implementing such dynamics remains far beyond the capabilities for the present generation Earth systems models. Several studies have found that in some ecosystems lack of N in soil usually leads to dominance of woody symbiotic ~~nitrogen~~ N fixers (e.g. Menge et al. , 2012). The availability of P is also impacted by the geochemical interactions in terrestrial soils, Vitousek et al. (2010) defined six mechanisms by which P is driven to limitation: loss by leaching, soil barriers that physically prevents access to roots, slow release of mineral P forms, P parent material, sequestration of P in soils and pools in the ecosystem and finally, anthropogenic input of nutrients.

Despite its importance P terrestrial limitation has been rare in Earth system modelling. The effect of P in tropical forest may be the key to better represent the vegetation biomass and the response to CO_2 fertilization. The lack of P observational data is in partly responsible for the difficulty of simulating P limitation in Earth system models (Spafford and MacDougall , 2021). However, several studies have attempted to provide reliable global P datasets (Yang et al. , 2013; Hartmann et al. , 2014; He et al. , 2021) that could be use to develop more accurate models. Furthermore, many studies have shown that the inclusion of P into ESM structures is possible and that it improves the representation of vegetation biomass in tropical regions (Wang et al. , 2007, 2010; Goll et al. , 2012, 2017; Fleischer et al. , 2019; Thum et al. , 2019; Yang et al. , 2019; Wang et al. , 2020; Nakhavali et al. , 2021). The addition of nutrient limitation has been observed to mainly effect the capacity of vegetation to uptake carbon (Wang et al. , 2010; Goll et al. , 2017; Wang et al. , 2020). Therefore, the accumulation of carbon in the atmosphere is enhanced, leading to increases of temperature in simulations. This temperature changes are likely to have some impact to variables sensitive to atmospheric temperature changes. Furthermore, the decrease of vegetation biomass affects variables affected by the distribution and composition of plant functional types, as changes in terrestrial albedo.

Intermediate complexity Earth system models, have a lower spatial representation, and model structures that have been intentionally simplified in one or more ways. This simplification allows for long-term simulations that are typically not feasible in higher complexity models. This class of model is not suitable for studying processes at small spatial scales. Hence, they are used in research questions that require large spatial and temporal scales (Weber , 2010). Current generation Earth system models are

or have already developed nutrient limitation to their model structure (e.g., Community Land Model (Lawrence et al. , 2019) , Joint UK Land Environment Simulator (Clark et al. , 2011), Community Atmosphere–Biosphere Land Exchange model (Haverd et al. , 2018), Australian Community Climate and Earth System Simulator (Ziehn et al. , 2020)). While CN models are more common CNP models remains to be rarer. However, P cycles have been suggested to be included into Earth system model for its importance in tropical regions (Wang et al. , 2010; Goll et al. , 2012). The first attempt to include nutrient limitation in the University of Victoria Earth system and climate model (UVic ESCM) was done by Wania et al. (2012) but was not included in the current publically available version of the model due to the need of further improvement. Hence, here We aim to describe a terrestrial N and P cycle adapted, developed and implemented for the UVic ESCM version 2.10. The main dynamics captured in this study are in the terrestrial system, especially vegetation. Furthermore, we intent to improve the current state of the previous N cycle implement in the UVic ESCM, develop a new P cycle and couple CNP in the UVic ESCMcarbon N and P, in order to improve the carbon cycle feedbacks projections.

2 Methodology

2.1 Model description

The UVic ESCM is a climate model of intermediate complexity (ver. 2.10, Weaver et al. (2001); Mengis et al. (2020)), it contains a simplified moisture-energy balance atmosphere coupled with a three-dimensional ocean general circulation (Pacanowski , 1995) and a thermodynamic sea-ice model (Bitz et al. , 2001). The model has a common horizontal resolution of 3.6° longitude and 1.8° latitude and the oceanic module has a vertical resolution of 19 levels with a varying vertical thickness (50 m near the surface to 500 m in the deep ocean).

In version 2.10, the soil is represented by 14 subsurface layers with thickness exponentially increasing with depth with a surface layer of 0.1 m, a bottom layer of 104.4 m and a total layer of 250 m. Only the first 8 layers have active hydrological processes (top 10 m), below that lays bedrock with thermal characteristics of granitic rocks. The soil carbon cycle is active in the top 6 layers up to a depth of 3.35 m (Avis , 2012; MacDougall et al. , 2012) the soil respiration is a function of temperature and moisture (Meissner et al. , 2003). The terrestrial vegetation is simulated by a top-down representation of interactive foliage and flora including dynamics (TRIFFID) representing vegetation interaction between 5 functional plant types: broadleaf trees, needleleaf trees, shrubs, C3 grasses, and C4 grasses that compete for space in the grid following the Lotka-Volterra equations (Cox , 2001). Net carbon fluxes estimated in the model updates the total areal coverage, leaf area inxes and canopy height for each PFT. For each PFT the carbon fluxes are derived from a photosynthesis-stomatal conductance model (Cox et al. , 1998). The carbon uptake though photosynthesis is allocated into growth and respiration and the vegetation carbon is transferred to the soil via litter fall and allocated in the soil as a decreasing function of depth (proportional to root distribution) and expect for the top layer is only added to soil layers with temperature above 1°C.

Furthermore, permafrost carbon is prognostically generated within the model using a diffusion-based scheme meant to approximate the process of cryoturbation (MacDougall and Knutti , 2016). The sediment processes are modelled using an oxic-only calcium carbonate scheme (Archer , 1996). Terrestrial weathering is diagnosed from the spin-up net sediment flux
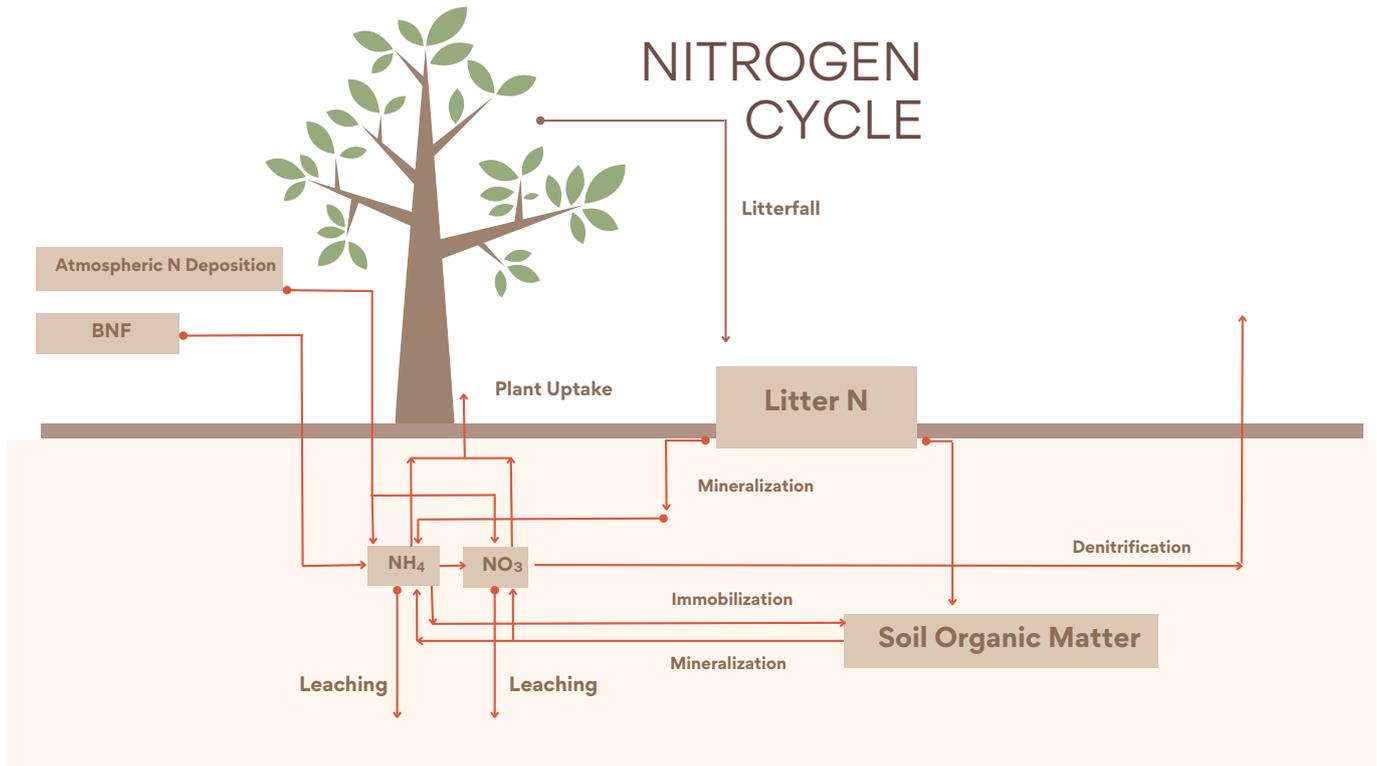
Figure 1. Diagram representing the UVic ESCM nitrogen cycle.

125   and stays fixes at the preindustrial equilibrium value (Meissner et al. , 2012). Mengis et al. (2020) merged previous version of the UVic ESCM and evaluated its performance representing carbon and heat fluxes, water cycle and ocean tracers. A full description of the model can be found in Mengis et al. (2020).

2.2   Nitrogen cycle

2.2.1   Nitrogen uptake

130   The new N cycle module was adapted from Wania et al. (2012). The module contains three organic (litter, soil organic matter and vegetation) and two inorganic (NH_4^+, NO_3^-) N pools. The base structure is based on Gerber et al. (2010) with further modifications to fit the UVic ESCM scheme. NH_4^+ is produced both from ~~Biological Nitrogen Fixation (BNF)~~ BNF and mineralization of organic ~~nitrogen~~N, it can be taken up by plants (vegetation), leached, or transformed into NO_3^- via nitrification. NO_3^- is produced through nitrification, can be taken up by plants, leached or denitrified into NO, N_2O or N_2.

135   The inorganic N is distributed between leaf, root and wood, with wood having a fixed stoichiometry ratio and variables ratios for the leaf and root pools. Organic N leaves the living pools via litter-fall into the litter pool which is either mineralized or

transferred to the organic soil pool, part of this N can be mineralized into the inorganic N pools. At the same time N can flow from the inorganic to the soil organic pool via immobilization. The CN ratios in leafs are determined by Eq. (1):

$$CN_{leaf} = \frac{C_{leaf}}{N_{leaf}}, \tag{1}$$

where C_{leaf} is the carbon content in leafs and N_{leaf} is the ~~nitrogen~~ N content in leafs. CN_{leaf} is one of the most important nutrient limitators in the model. It controls the maximum carboxilation rate of RuBISCO. Furthermore, it control vegetation biomass. If ~~nitrogen concentration in leafs~~ leaf C:N ratio is higher than $CN_{leafmax}$ (the maximum CN ratio parameter) terrestrial vegetation biomass is reduced.

The new version of the N cycle has been merged with a deep land-surface (MacDougall and Knutti , 2016) and a new wetland module (Nzotungicimpaye et al. , 2021). Both inorganic N pools are transferred between soil layers following ground-water flow. Given this flow the distribution of N in layers was taken into account in the uptake calculations in Eq. (2) and (3), a root fraction was added (4) fixing the amount of root biomass per PFTs per layer depth. The equations governing N uptake are:

$$NH_4^{UP} = \sum_{PFT} \left(\frac{V_{maxn}C_{root}\left[NH_4\left(av\right)\right]Froot}{K_{n,1/2} + \left[Nmin\left(av\right)\right]} + \left[NH_4\left(av\right)\right] * Qt\right), \tag{2}$$

$$NO_3^{UP} = \sum_{PFT} \left(\frac{V_{maxn}C_{root}\left[NO_3\left(av\right)\right]Froot}{K_{n,1/2} + \left[Nmin\left(av\right)\right]} + \left[NO_3\left(av\right)\right] * Qt\right), \tag{3}$$

where NH_4^{UP} and NO_3^{UP} represent the ~~nitrogen~~ N uptake, the left term is the active uptake while the right term is the passive uptake (see table 1), the latter is the transport of N via the transpiration water stream. $Vmaxn$ is the ~~maximun~~ maximum uptake rate for ~~nitrogen~~N, $Croot$ is the root carbon biomass, $[NH_4(av)]$, $[NO_3(av)]$ and $[Nmin(av)]$ are the NH_4, NO_3 and mineral ~~nitrogen~~ N concentrations, $K_{n,1/2}$ is the half saturation constant for ~~nitrogen~~ N and Qt is the transpiration rate. av represents the available portion of NH_4 and NO_3 in soil. This fraction is calculated as the total concentration of NH_4 and NO_3 divided by sorption factors (10 and 1 respectively) following Wania et al. (2012). The equation for root fraction is:

$$Froot,_{PFT} = \frac{e^{z_{top,n}/d_{r,PFT}} - e^{z_{bot,n}/d_{r,PFT}}}{1 - e^{D/d_{r,PFT}}}, \tag{4}$$

where Z_{top} and Z_{bot} represents the top layer and bottom layer depth respectively, while D and d_r are the depth of the soil layer and the root depth. The depth of soil layer represents the depth of each specific soil layer. Root depth is a PFT based parameter that represents the depth of the roots. Given the multiple soil layer set up, the root fraction modifies the value of root carbon, creating a more realistic representation of the uptake root depth reach for each PFT given the multiple soil layer set up.

2.2.2 Denitrification

The N cycle was merged with a wetland module that allowed the estimation of anoxic fractions for each soil layer, based on Gedney and Cox (2003). The anoxic fraction is taken to be the saturated fraction of the soil layer that is shielded from O_2

by the saturated soil layer above. The Anoxia representation led to denitrification to be added to the N model, accounting the largest exit pathway for N in the terrestrial biosphere. The anaerobic respiration is estimated from eq. (5):

$$R_{an} = K_{rNO3} f_t f_m C_s A_f \frac{[NO_3(av)]}{[NO_3(av)] + K_n},\tag{5}$$

where R_{an} is the anaerobic respiration, K_{rNO3} is the ideal respiration rate via NO_3 reduction, f_t and f_m are temperature and moisture functions, C_s is the concentration of organic carbon, Af is the anaerobic fraction, K_n is the half-saturation of N-oxides (Li et al. , 2000). The temperature and moisture soil functions are taken directly from Cox (2001), and are represented by the following equations:

$$f_t = q_{10}^{0.1(t_s - 25)},\tag{6}$$

$$f_m = \begin{cases} 1 - 0.8(S - S_0) & \text{for S} > S_0, \\ 0.2 + 0.5(\frac{S - S_W}{S_0 - S_W}) & \text{for } S_W < S \leq S_0, \\ 0.2 & \text{for S} \leq S_W, \end{cases}\tag{7}$$

where in f_t, q_{10} = 2 and t_s is the soil temperature in °C. In f_m, S is the soil moisture, S_W is the wilting point of soil moisture, S_0 is the optimum soil moisture. Fluxes of N_2O and NO to the atmosphere are computed based on the 'leaky-pipe' conceptualization of soil-nitrogen processes (Firestone and Davidson , 1989). In the leaky pipe conceptual model N_2O and NO leak out of reactions of one species of nitrogen into another, namely nitrification (NH_4 to NO_3) and denitrification (NO_3 to N_2). The size of the holes is determined by the soil processes. For implementation in the UVic ESCM the size of the holes is fixed but the partitioning ratio between NO and N_2O changes based on water filled pore space of the soil layer. The ratio is parameterized based on an empirical relationship derived by Davidson et al. (2000):

$$\frac{N_2O}{NO} = 10^{2.6 S_U - 1.66},\tag{8}$$

where S_U is the water filled pore space. Thus, the model produces a total flux of both NO and N_2O for nitrification and denitrification, which is partitioned between the two species based on the above relationship. The NO flux is added to the atmosphere and redeposited as part of the ~~nitrogen~~ N deposition flux. The N_2O flux is added to the N_2O pool in the atmosphere which has a characteristic half-life of 90.78 years ~~Myhre et al. (2013)~~(Myhre et al. , 2013). Decayed N_2O is assumed to become part of the atmospheric N_2 pool.

2.2.3 Mass balance N cycle

In Wania et al. (2012) ~~nitrogen~~ N cycle module, under N limitation ($CN_{leaf} > CN_{leafmax}$) the N available was increased artificially by reducing the leaching by up to 100% and if necessary the immobilization by 50%. These mechanics created an
190   unrealistic increase of N in soils and thereby, defying the mass balance conservation of the module.

     Here, the vegetation can no longer uptake extra N from leaching or immobilization under nutrient limitation. Instead, under nutrient limitation wood and root carbon mass is transferred as litter (emulating a dying vegetation) until the correct ratio is met. Section 2.4 presents a detailed explanation of nutrient limitation for N and P.

Table 1. Updated nitrogen cycle module pools, rates and variables.

Variables	Units	Type	Descriptions
NH_4^{UP}	kg N m^{-2} yr^{-1}	Rate	NH_4 vegetation uptake
NO_3^{UP}	kg N m^{-2} yr^{-1}	Rate	NO_3 vegetation uptake
Croot	Kg C m^{-2}	Pool	Root carbon
$[NH_4(av)]$	kg N m^{-3}	Pool	Available NH_4 concentration
$[NO_3(av)]$	kg N m^{-3}	Pool	Available NO_3 concentration
Froot	-	Variable	Root fraction
$[Nmin(av)]$	kg N m^{-3}	Pool	Available mineral N concentration
R_{an}	kg C m^{-3} s^{-1}	Rate	Anaerobic respiration rate
C_s	kg C m^{-3}	Pool	Density of soil carbon in each layer
A_f	-	Variable	Anaerobic saturation fraction
N_2O	kg N m^{-2} yr^{-1}	Rate	Nitrous oxide flux
NO	kg N m^{-2}yr^{-1}	Rate	Nitric oxide flux

2.3 Phosphorus cycle

195   The P cycle is based on Wang et al. (2007, 2010) and Goll et al. (2017) with some equations where modified from Wania et al. (2012) to have a better consistency with N estimations in the new soil layer model. The module contains four inorganic (labile, sorbed, strongly sorbed and occluded) and three organic P pools: Vegetation (leaf, root and wood), litter and soil organic P.

2.3.1 Input

The P module estimates weathering input following Wang et al. (2010) and is driven by a fixed estimate (Table 3) of P release
200   assigned by soil order divided in 12 classes from U.S. department of agriculture (USDA) soil order map.

     Additionally, an extra input structure was tested in the model but was not used for the P results in this study. It was implemented to compare the benefits of a static and a dynamic weathering scheme into the P pool. In this method weathering

Table 2. Updated nitrogen cycle parameters. See appendix A.1 for values that vary for each PFT.

Variables	Units	Value	Description	Source
$K_{n,1/2}$	kg N m^{-3}	0.003	Half saturation constant for N uptake	Gerber et al. (2010)
$Vmaxn$	kg N (kg root C^{-1})yr^{-1}	Varies with PFTs	Maximun uptake rate for N	Wania et al. (2012)
D	m	Varies with soil layer	Soil layer depth	MacDougall and Knutti (2016)
Qt	m yr^{-1}	Varies with PFTs	Transpiration rate	Wania et al. (2012)
$z_{top,n}$	m	Varies with soil layer	Top layer soil depth	Avis (2012)
$z_{bot,n}$	m	Varies with soil layer	Bottom soil layer depth	Avis (2012)
d_r	m	Varies with PFTs	Root depth	Avis (2012)
K_{rNO_3}	10^{-9} s^{-1}	5	Soil respiration rate for Nitrate respiration	
K_n	kg N m$_{-3}$	0.083	Half saturation constant for N-oxides	Li et al. (2000)
$CN_{leafmax}$	kg C (kg N)$^{-1}$	Varies with PFTs	Maximum CN ratio	Wania et al. (2012)

Table 3. Constants for P input from Wang et al. 2010. The values change depending on the weathering state of the soil type. Highly weathered soils have lower values.

Soil order	Value (gP m^{-2} yr^{-1})
Entisol	0.05
Inceptisol,Gellisol,Histosol	0.05
Vertisol	0.01
Aridisol,Andisol	0.01
Mollisol	0.01
Alfisoil,Spodosol	0.01
Ultisoil	0.005
Oxisoil	0.003

depends on runoff following Hartmann et al. (2014) using the lithological world map with 16 different classes generated by Hartmann and Moosdorf (2012). Eq. 9 shows the estimation of the chemical weathering rate:

205 $$F_{CW} = b_i q, \tag{9}$$

$$b_i = b_{carbonate} + b_{silicate}, \tag{10}$$

where F_{CW} (t km^{-2} yr^{-1}) is the chemical weathering rate, q is the runoff (mm yr^{-1}) and b_i is the factor for each lithological class i; shielding correction functions were not applied. The chemical weathering is defined as the total fluvial export of Ca
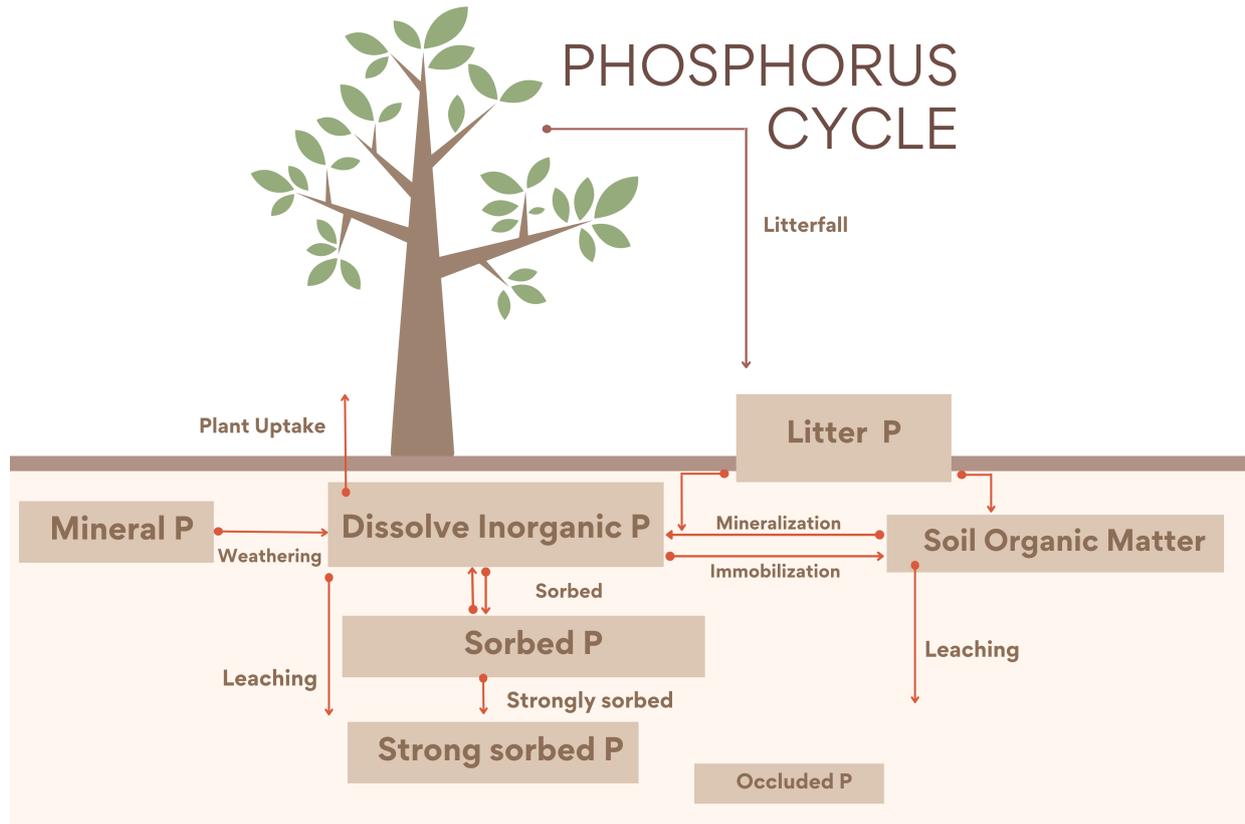
Figure 2. Diagram representing the UVic ESCM CNP ~~phosphorus~~ P cycle. Weathering from mineral P is the only input into the soils. There are 4 inorganic pools (Dissolved inorganic, adsorbed , stronged sorbed and occluded P) and 3 organic pools (vegetation (root, wood and leaf), litter and soil organic matter). As in Wang et al. (2010) the flux from strongly sorbed P to the occluded pool is not represented here, instead it is assumed to be a fraction of total soil P.

+ Mg + K + SiO$_2$ and carbonate derived CO$_3$, b$_{carbonate}$ and b$_{silicate}$ are chemical weathering parameters associated to carbonate and silicate rocks respectively found in Hartmann et al. (2014). Here we only apply Wang et al. (2010) approach as we found it to be more controllable and an advantage to the planned coupling of P flux from land into the ocean. Hartmann et al. (2014) requires the estimation of runoff by the model structure. Hence, while representing a dynamical P release it needs to be carefully assessed so that no extreme overestimation or underestimation are represented regionally. Wang et al. (2010) approach provides constant input without variability which in this particular case is favorable.

2.3.2 Inorganic soil phosphorus

Inorganic P (Psoil) in soil follows the dynamics described in (Goll et al. , 2017) in eq. (11), where each time step a fix fraction (k$_s$) of P is adsorbed and the rest is dissolved (1-k$_s$). This fraction is based on Hedley fractionation method (Hedley and

Stewart , 1982) which is dependant on soil orders, the dataset has been commonly used to assess the different P forms in soil. The adsorbed P is regulated by k_s in eq. (12) as determined by the soil order in Hedley dataset:

$$220 \quad \frac{dPsoil}{dt} = (1 - K_s)(P_{wea} + P_{litmin} + P_{orgmin} - P_{leach} - P_{up} - \tau_{sorb}P_{sorb} - P_{imm}), \tag{11}$$

$$\frac{dPsorb}{dt} = K_s \frac{dPsoil}{dt}, \tag{12}$$

where P_{wea} is the P released by rock weathering, P_{litmin} is the P mineralized from the P litter pool, P_{orgmin} is the P mineralized from the soil organic P, P_{leach} is the leached inorganic P, P_{up} is the P uptake by plants, P_{sorb} is the amount of P sorbed, τ_{sorb} is the rate of strong sorption and P_{imm} is the P immobilized from the inorganic P pool. The estimation of $Psoil$

225 based on Goll et al. (2017), is originally taken from Goll et al. (2012). Here, the sum P_{sorb} and P_{soil} constitute the inorganic P pool in soil. Hence, the loss given by the rate of strong sorption is applied to the total inorganic P pool. The estimation of occluded P followed Wang et al. (2010) approach, based in Cross and Schlesinger (1995) the pool was assumed to be 35 % of the total soil P. P_{leach} and P_{up} were determined as in eq. (13), (14) based on an adaptation of Wania et al. (2012) representation of leaching and uptake of N in the new soil layer model version:

$$230 \quad P_{leach} = Q_D P_{soil}, \tag{13}$$

$$P_{UP} = \sum_{PFT} \left(\frac{V_{maxp}C_{root}[P_{soil}]F_{root}}{K_{p,1/2} + [P_{soil}]} \right), \tag{14}$$

where Q_D is the runoff. V_{maxp} is the P maximum uptake rate, $K_{p,1/2}$ is the half saturation constant for P, C_{root} is the root carbon and F_{root} is the root fraction.

2.3.3 Organic soil phosphorus

235 After uptake, P is distributed in three vegetation compartments: leaf, root and wood. Leaf and root have a dynamic value that varies between a minimum and a maximum, while wood have a fix CP ratio. The vegetation P biomass dynamics is determined from the difference between the amount of uptake and the loss from litterfall as in eq. (15) and the litterfall is estimated as the CP ratio of the original model litterfall as in eq. (16):

$$\frac{dVegp}{dt} = P_{UP} - P_{LF}, \tag{15}$$

$$240 \quad P_{LF} = \sum_{PFT} \frac{Lit_{leaf}}{CP_{leaf}}(1 - R_{leafp}) + \frac{Lit_{root}}{CP_{root}} + \frac{Lit_{wood}}{CP_{wood}}, \tag{16}$$

where V_{egp} is the vegetation P change over time, P_{LF} is the P litterfall and Lit_{leaf}, Lit_{root}, Lit_{wood} are the carbon litterfall rates for vegetation carbon. The leaf CP ratio is determined as:

$$CP_{leaf} = \frac{C_{leaf}}{P_{leaf}}, \tag{17}$$

where C_{leaf} is the carbon content in leafs and P_{leaf} is the P content in leafs. CP_{leaf} is one of the most important nutrient limitators in the model. The limiting effect of CP_{leaf} is when its value is higher than the maximum CP ratio parameter $CP_{leafmax}$. This leads to biomass reduction. In contrast to CN_{leaf}, CP_{leaf} does not control the maximum carboxilation rate of RuBISCO. A more detailed description of nutrient limitation can be found in section 2.4. The litter biomass is added to the P litter pool (P_{lit}), its dynamic is based on Wang et al. (2007) as in eq. (18):

$$\frac{dP_{Lit}}{dt} = P_{LF} - \tau_{lit} P_{lit} - P_{litmin}, \tag{18}$$

$$P_{litmin} = \frac{P_{lit}}{P_{som} + P_{lit}} P_{tase}, \tag{19}$$

$$P_{tase} = U_{tase} \frac{\lambda_{up} - \lambda_{UPtase}}{\lambda_{up} - \lambda_{Ptase} + K_{ptase}} \frac{\lambda_{up} - \lambda_{Ptase}}{\lambda_{up} - \lambda_{Ptase} + K_{ptase}}, \tag{20}$$

where τ_{lit} is a rate constant for litter carbon decomposition (0.42 yr^{-1}), P_{litmin} is the biochemical P litter mineralization, P_{tase} is the biochemical P mineralization rate, U_{tase} is the maximum rate of P biochemical mineralization, λ_{up} is the N plant root cost to uptake P, λ_{Ptase} is the critical value of N cost of root P uptake above which phosphate production starts and K_{ptase} is the Michaelis-Menten constant for biochemical P mineralization. Here, the N cost refers to the N required for protein structures involved in the metabolization of P in plants. P_{tase} is a constant value.

The soil litter decomposed is transferred to the soil organic P pool (P_{som}); the dynamics of P_{som} are adapted from Wang et al. (2007) as in eq. (21):

$$\frac{dP_{som}}{dt} = \tau_{lit} P_{lit} \varepsilon - \tau_s P_{som} - P_{orgmin}, \tag{21}$$

$$P_{orgmin} = \frac{P_{som}}{P_{lit} + P_{som}} P_{tase}, \tag{22}$$

where the first term represents the litter P input, while the other two are the P_{som} decomposition and mineralization. ε is a microbial growth efficiency (0.6), τ_s is the rate constant for soil carbon decomposition and P_{orgmin} is the biochemical P mineralization. The immobilization is determined from the NP ratio of the N immobilization estimated by Wania et al. (2012).

2.4 Nitrogen and phosphorus limitation

The ~~nitrogen~~ N cycle limits the terrestrial vegetation productivity in two distinct ways: the first limits the photosynthesis efficiency by controlling the maximum carboxylation rate of Rubisco (V_{cmax}). The Rubisco enzyme plays a crucial role in the photosynthesis biochemistry by catalysing the carboxylation reactions in the Calvin cycle and has been found to be linearly related to the ~~nitrogen~~ N leaf content (Walker et al. , 2014). The original equation for V_{cmax} takes into account a fix N leaf (Cox et al. , 1999), this was replaced by Wania et al. (2012) implemented in the first N cycle where it is replaced by the calculated inverse average canopy leaf C/N ratio ($CN_{invleaf}$), in this representation the plant productivity is reduced when CN_{leaf} increases. V_{cmax} is calculated as:

$$V_{cmax} = \lambda CN_{invleaf}, \tag{23}$$

where λ is a constant of proportionality, 0.004 for C3 and 0.008 for C4 PFTs (Cox et al. , 1999). ~~Nitrogen and phosphorus~~ N and P both share the second form of limitation, where stoichiometrically N and P limitation reduce the vegetation biomass. If C:N ratios is too high wood and root carbon biomass is transferred to the litter pool until the normal C:N ratio is reached (See table 4).

The model assumes nutrient limitation when the ~~concentration of nitrogen and phosphorus~~ estimated CN and CP leaf ratio is higher than the maximum CN ($CN_{leafmax}$) and CP ($CP_{leafmax}$) ratio in leafs. For grids with nutrient limitation the carbon in leaves is reduced to match the maximum CN or CP ratios in leafs. The carbon that is reduced is transferred to the litter pool. This reduction can happen for one or both nutrients until the ratio is met. The following equations regulate the reduction of biomass based on nutrient limitation:

$$C_{leaflimitedn} = N_{leaf}CN_{leafmax}, \tag{24}$$

$$C_{leafdiffn} = C_{leaf} - C_{leaflimitedn}, \tag{25}$$

$$C_{leaflimitedp} = N_{leaf}CP_{leafmax}, \tag{26}$$

$$C_{leafdiffp} = C_{leaf} - C_{leaflimitedp}, \tag{27}$$

where $C_{leaflimitedn}$ and $C_{leaflimitedp}$ are the carbon concentration in leafs if the system is considered to be limited. $C_{leafdiffn}$ and $C_{leafdiffp}$ are the the carbon lost due to nutrient limitation and their value are sum in the litterfall equation when the system is in nutrient limitation.

Table 4. Maximum leaf C:P and C:N in the CNP simulation by PFTs.

Variables	Broadleaf trees	Needleleaf trees	C3	C4	Shrubs
$CP_{leafmax}$	225	250	500	500	450
$CN_{leafmax}$	70	80	60	80	80

2.5 Model runs and validation

The three different terrestrial biogeochemical versions: C, CN and CNP, were run for a historical simulation from 1850 to
295 2020. The C version served as a baseline run representing the original version of the UVic ESCM ver. 2.10 (Mengis et al. ,
2020), the CN version is the modified version of Wania et al. (2012) N model, and CNP is newest coupled model that includes
~~phosphorus~~P. Historical simulations are forced with fossil CO_2 emissions, dynamically determined land use change emissions,
non-CO_2 GHG forcing, sulfate aerosol forcing, volcanic anomalies forcing, and solar forcing. Furthermore, 24 historical sim-
ulations were run to assess model sensitivity of 6 key parameters ($CP_{leafmax}$, $CN_{leafmax}$, R_{leafp}, R_{leafn}, V_{maxp}, V_{maxn}) in
300 N and P limitation over terrestrial vegetation. The parameters were perturbed by increasing and reducing their value by 10 %
and 20 % individually. $CP_{leafmax}$ and $CN_{leafmax}$ are the maximum leaf CP or CN ratios respectively. If the values of CP_{leaf}
and CN_{leaf} are above these thresholds the model will take the system to be nutrient limited by either P or N. R_{leafN} and
R_{leafP} are parameters that represents the resorption of ~~nitrogen and phosphorus~~ N and P in leafs. This partly controls the loss
of ~~nitrogen and phosphorus~~ N and P from vegetation to the litter pool. V_{maxp} and V_{maxn} are the P and N maximum uptake
305 rates.

It should to be noted that the porting of the N cycle from version 2.9 to 2.10 of the UVic ESCM and later model spin-up,
could slightly alter the results presented in Mengis et al. (2020). Hence, our baseline model is slightly different from the
standard UVIC ESCM ver. 2.10. The ~~nitrogen~~ N cycle is compared to Zaehle et al. (2010); Li et al. (2000) and Yang et al.
(2009) as well as Wania et al. (2012). The N_2O flux was compared with the Emissions Database for Global Atmospheric
310 Research (EDGAR ver. 6.0, Crippa et al. (2021)) dataset, it provides emission time series from 1970 until 2015 for non-CO2
GHGs for all countries.

For the P cycle, we used as benchmark for the carbon cycle the UVic ESCM version 2.10 model calibration values and
references, which included the Le Quere et al. (2018) datasets. The total soil ~~phosphorus~~ P was calibrated with the He et al.
(2021) dataset. The labile and sorbed pools were calibrated using Yang et al. (2013) P distributions map dataset. For the use
315 of He et al. (2021) dataset we transformed the units with Eq. 28:

$$P_{soil} = Bk_{density} * SL_D * P_{dataset}, \tag{28}$$

where P_{soil} is the total P soil concentration (kg P m^{-2}), $Bk_{density}$ (kg m^{-3}) is the builk density taken from International
Geosphere-Biosphere Programme Data and Information System (IGBP-DIS) (Global Soil Data Task Group , 2014), SL_D (m)

is the soil layer depth and $P_{dataset}$ (kg P (kg soil)-1) is He et al. (2021) dataset. The foliar stochiometry was compared to the latitudinal trend from Reich and Oleksyn (2004) N:P observations.

One of the challenges of modelling nutrients in terrestrial systems is the lack of observations and validation datasets. Furthermore, the existing range of values for N and P variables are highly uncertain. This large range in values makes it difficult to accurately tune models. Although, improvements are in sight, with new artificial intelligence derived global datasets beginning to become available (He et al. 2021). Model validation has been advancing quickly in the last decade (Spafford and MacDougall , 2021) with tools such as the International Land Model Benchmarking (Collier et al. , 2018) that significantly improves terrestrial model validation. However, there are limited variables available to compare to nutrient model development. The increase of the addition of nutrient structures in ESMs (Arora et al. , 2020) suggest the need of terrestrial nutrient validation tools to improve model accuracy in the developmental phase. Moreover, a terrestrial nutrient model intercomparison project would unify global efforts to improve the representation of N and P in ESMs.

Table 5. Phoshorus cycle model pools and variables.

Variables	Units	Descriptions
P_{litmin}	kg P m^{-2} yr^{-1}	P litter mineralization
P_{orgmin}	kg P m^{-2} yr^{-1}	P organic matter mineralization
P_{leach}	kg P m^{-2} yr^{-1}	P leaching
P_{up}	kg P m^{-2} yr^{-1}	P uptake
P_{sorb}	kg P m^{-2} yr^{-1}	P sorption
P_{imm}	kg P m^{-2} yr^{-1}	P immobilization
$[P_{soil}]$	kg P m^{-3}	Soil layers labile P concentration
P_{soil}	kg P m^{-2}	Labile ~~phosphorus~~P
Lit_{leaf}	kg C m^{-2} yr^{-1}	Leaf literfall rate
CP_{leaf}	kg C (kg P)$^{-1}$	CP leaf ratio
Lit_{root}	kg C m^{-2} yr^{-1}	Root literfall rate
CP_{root}	kg C (kg P)$^{-1}$	CP root ratio
Lit_{wood}	kg C m^{-2} yr^{-1}	Wood literfall rate
CP_{wood}	kg C (kg P)$^{-1}$	CP wood ratio
F_{tase}	kg P m^{-2} yr^{-1}	Rate of P biochemical mineralization
P_{som}	kg P m^{-2}	P soil organic matter pool
P_{lit}	kg P m^{-2}	P litter pool

Table 6. Phosphorus cycle model parameters.

Variables	Units	Value	Description	Source
K_s	-	Varies with soil order	Fraction of P sorbed	Goll et al. (2017)
P_{wea}	kg P m^{-2} yr^{1-}	Varies with soil order	~~Phosphorus~~ P flux from weathering	Wang et al. (2010)
τ_{sorb}	yr^{-1}	0.067	Rate of P strong soil sorption	Wang et al. (2010)
$K_{p,1/2}$	kg P m^{-3}	0.002	Half saturation constant for P uptake	Machado and Furlani (2004)
V_{maxp}	kg P (kg root C^{-1})yr^{-1}	0.46	Maximum uptake rate for P	Tuned
R_{leaf}	-	0.5	Leaf P readsorption rate	Tuned
U_{tase}	kg P m^{-2} yr^{-1}	0.0001	Maximum biochemical mineralization rate	Wang et al. (2007)
λ_{up}	kg C (kg P)$^{-1}$	25	N cost of plant root P uptake	Wang et al. (2007)
λ_{ptase}	kg C (kg P)$^{-1}$	15	Critical N cost of root P uptake	Wang et al. (2007)
K_{ptase}	kg C (kg P)$^{-1}$	150	Constant for biochemical P mineralization	Wang et al. (2007)
τ_{lit}	yr^{-1}	0.42	Rate constant for litter C decomposition	Wang et al. (2007)
ε	-	0.6	Microbial growth efficiency	Wang et al. (2007)
τ_s	yr^{-1}	0.02	Constant for soil carbon decomposition	Wang et al. (2007)
λ	-	Varies with PFTs	Constant of proportionality	Cox et al. (1999)
$CP_{leafmax}$	kg C (kg P)$^{-1}$	Varies with PFTs	Maximum CP ratio	Tuned

3   Results and Discussions

3.1   Carbon cycle

3.1.1   Land global primary productivity

The global gross productivity in CN and CNP resulted in a better agreement with the FLUXCOM GPP dataset (Jung et al. , 2019) as shown in Fig. 3, with both CN and CNP overestimating the terrestrial global GPP average less than the baseline simulation. Compared to the baseline simulation (143 Pg yr^{-1}) both nutrient limited model versions showed a reduced mean GPP from the ~~year 2010-2020~~ years 2001-2015 with CN at 130 Pg yr^{-1} and CNP at 127 Pg yr^{-1}. Furthermore, the modifications for the N cycle in regards with the mass balance changes resulted in the reduction of mean GPP from 129 Pg yr^{-1} (Wania et al. , 2012) to 122 Pg yr^{-1} in the 1990s. The GPP distribution from Baseline, CN and CNP reproduce FLUXCOM dataset values reasonably well (Fig. 4). The seasonal pattern of GPP is also well represented within out simulations as shown in Fig. 4. The addition of nutrients improves the representation of GPP, where CNP had the highest correlation with FLUXCOM GPP dataset. The high GPP in the baseline simulation can be explained by the overestimation of the vegetation biomass especially broadleaf trees in tropical regions stated in Mengis et al. (2020). The representation of vegetation biomass is linked to the PFTs fractions in the model. In the CN and CNP simulations the reduction of biomass is critical for the reduction of terrestrial productivity, especially in tropical regions where P availability has been shown to be a limiting factor for GPP (Du et al. , 2020). Similar to Wania et al. (2012), Bonan and Levis (2010), and Zaehle et al. (2010) the addition of nutrient limitation in ESM seems to reduce GPP. Furthermore, locally in Amazonia soils, Nakhavali et al. (2021) found that the inclusion of ~~phosphorus~~ P reduces the model GPP and NPP outputs by 5.1 and 4.5% respectively for a site simulation. Similar to Nakhavali et al. (2021) we found an overall reduction of GPP in the Amazon region.

The nutrient limitation reduced the amount of land-atmosphere carbon flux in the simulations. The cumulative land uptake from 1850-2005 was 150 Pg C yr^{-1} in CNP, lower than version 2.10 calibration in Mengis et al. (2020) (177 PgC yr−1). This change in response is crucial for understanding the future dynamics in the Shared Socio Economic Pathways Projections as terrestrial vegetation is expected to decrease its capacity to store carbon in the future (Goll et al. , 2012). Overall, the carbon feedback values are in concordance with the ranges of the global carbon project used in Mengis et al. (2020) (Le Quere et al. , 2018) where the cumulative carbon flux was estimated to be 141 PgC yr^{-1} from 1850-2005. The atmosphere to land carbon flux follow the the GCP dataset (Le Quere et al. , 2018) magnitude closely.

Similar to Wania et al. (2012), we found higher values of NPP for CN (77.4 Pg C yr^{-1}) compared to the baseline simulation (74.2 Pg C yr^{-1}). While CNP (72 Pg C yr^{-1}) resulted in lower values, due to the reduction of tropical vegetation biomass. CN and CNP results are close to the upper range (21.5 to 69.3 Pg C yr^{-1}) of simulated NPP showed in Li et al. (2015). The reduction of tropical biomass mainly in broadleef trees carbon is reflected in the fraction of the PFT shown in the model output. Wania et al. (2012), argued that the reason behind the high NPP was the dependence of autotrophic respiration on N content in leaf, root and stem which are based on the original MOSES/TRIFFID version (Cox et al. , 1999). In CN and CNP, the reduction of wood CN ratios and higher leaf content than in CN and CNP which fluctuates from a minimum to a maximum
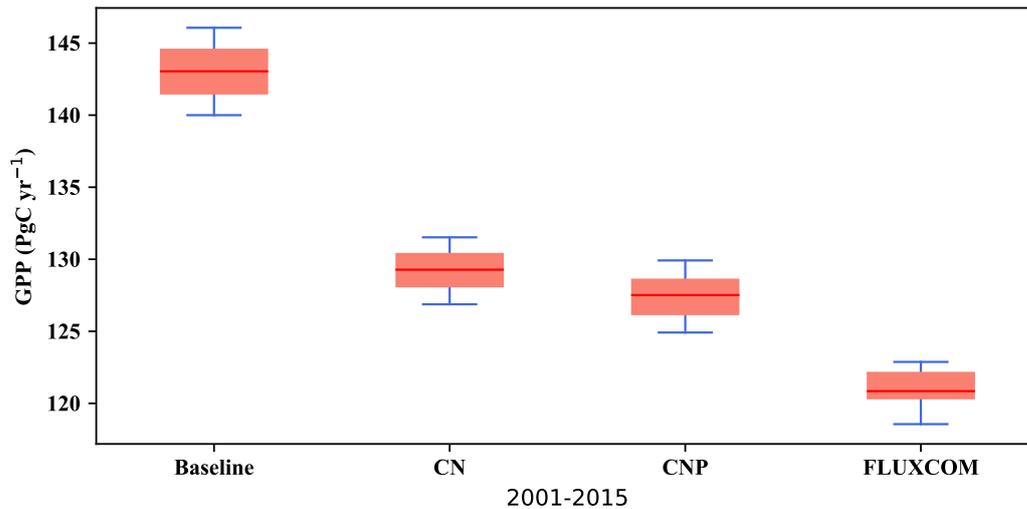
Figure 3. Modelled yearly Gross Primary Productivity (GPP) from 2001 to 2015 versus FLUXCOM GPP dataset (Jung et al. , 2019).

value gives place to the reduction of the maintenance respiration which reduces the autotrophic respiration and consequently NPP. Furthermore, in the new CNP version while wood CN remains to be fixed the stochiometrical reduction of wood carbon
365   by the lack of P availability decreases wood carbon even more especially in tropical forests and other tropical ecosystems.

3.1.2   Atmospheric CO_2 concentration

The simulated CNP atmospheric CO_2 concentration matches observations very closely and the addition of N and P has shown an improvement in the representation of the model accumulation of carbon in the atmosphere. The CO_2 concentration has improved compared to the evaluated 2.10 version of the UVic ESCM where from 1960 to 2010 the simulation deviates above
370   the observed curve (Δ78 ppm in the simulation compared to Δ73 ppm observations; Mengis et al. (2020)). Compared with the CN and baseline simulations (Fig. 3), CNP provides a more accurate representation of the atmospheric CO_2 concentration. Thus the nutrient limitation has effectively reduced the CO_2 fertilization effect on the terrestrial vegetation. Consequently, the CN and CNP show a larger pool of atmospheric CO_2.

3.1.3   Terrestrial vegetation

375   Given that tropical forests and savannas are commonly limited by the availability of P, the simulated vegetation biomass representation is affected by the absence of nutrient limitation in ESMs. Nakhavali et al. (2021) found that the addition of P improved the vegetation estimations and the carbon cycle response to rising CO_2 for the Amazonian region, basing their study in a site representative for 60% of the Amazon soils.
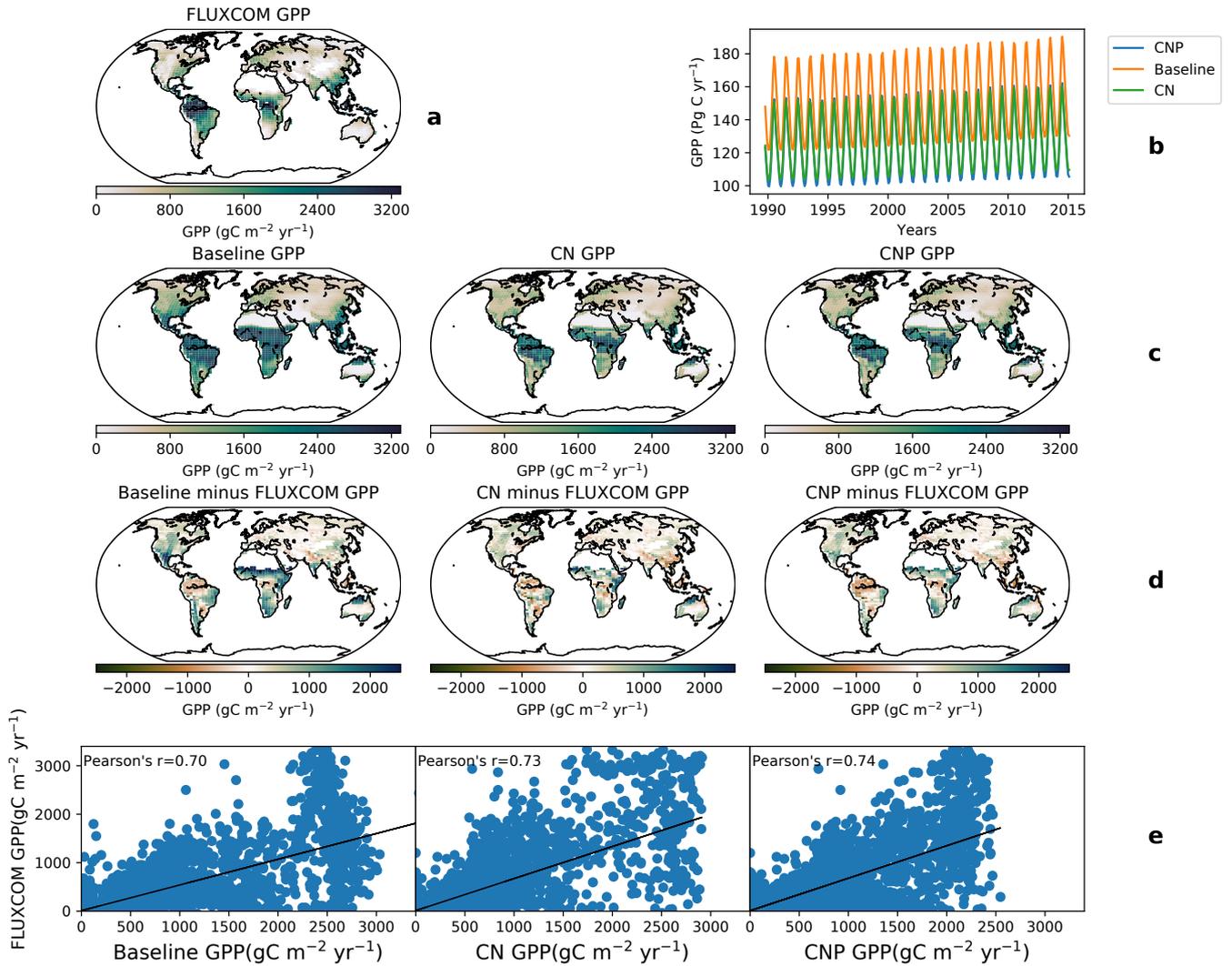
Figure 4. ~~Upper left figure shows~~ a. FLUXCOM GPP dataset from 2000-2010, ~~upper right figure shows the seasonal~~ b. Seasonal GPP from 1990-2015 for Baseline, CN and CNP. ~~The second~~ c. Second line ~~from left to right~~ shows the global GPP from 2000-2010 for Baseline, CN and CNP. d. The third line ~~from left to right~~ shows the difference between Baseline, CN and CNP and FLUXCOM GPP dataset. ~~The fourth line from left to right shows~~ e. Shows the correlation of Baseline, CN and CNP to FLUXCOM GPP dataset.
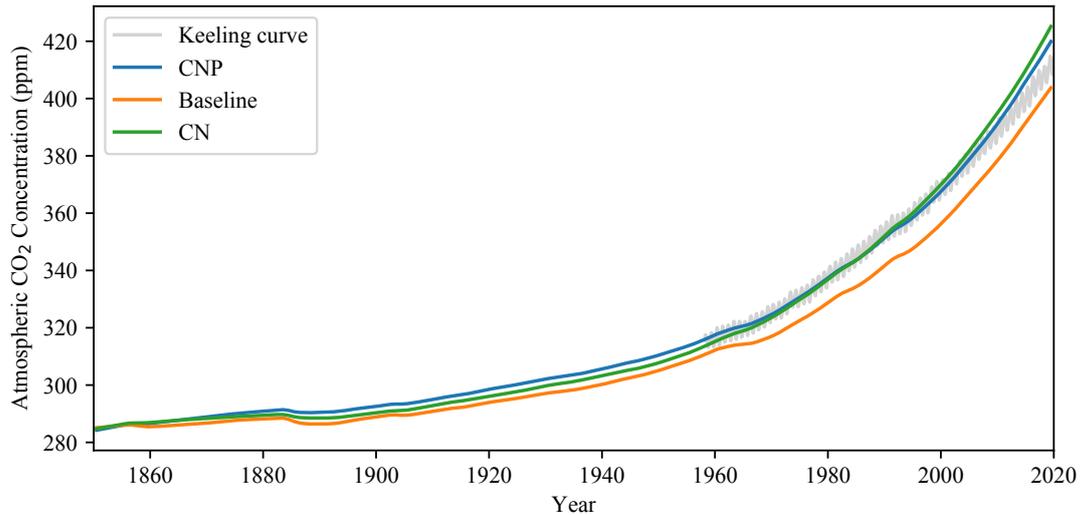
Figure 5. Atmospheric CO_2 concentration in CNP, CN and baseline simulations compared to the keeling curve from the Mauna Loa observatory (Keeling et al., 2005; grey line).

In the CNP version of the model Broadleaf trees coverage declined in tropical and subtropical latitudes (Fig. 6) with the largest changes located in South East Asia, Africa and South America. The reduction of vegetation biomass ranged from 6-20 % in South America and Africa, while a higher reduction of 20-30% was present in South Eastern Asia. The magnitude of continental difference can be attributed with the base internal vegetation biomass model version bias (Mengis et al. , 2020). Additionally, CN and CNP show a shift of coverage where broadleaf trees is taken over by C3 grass.

~~In the case of needleleaf trees this shift is observed to happen~~ Needleleaf trees were reduced in North America and Europe. Both CN and CNP simulations vegetation carbon resulted in a decrease of vegetation biomass with 456 Pg C and 525 Pg C respectively compared to baseline simulation (594 Pg C), similar to Zaehle et al. (2010). Overall CNP shows a high correlation with all PFTs coverage when compared with Poulter et al. (2015) PFTs dataset. In tropical regions our model seems to represent vegetation closely to the data (Fig. 7, 8).
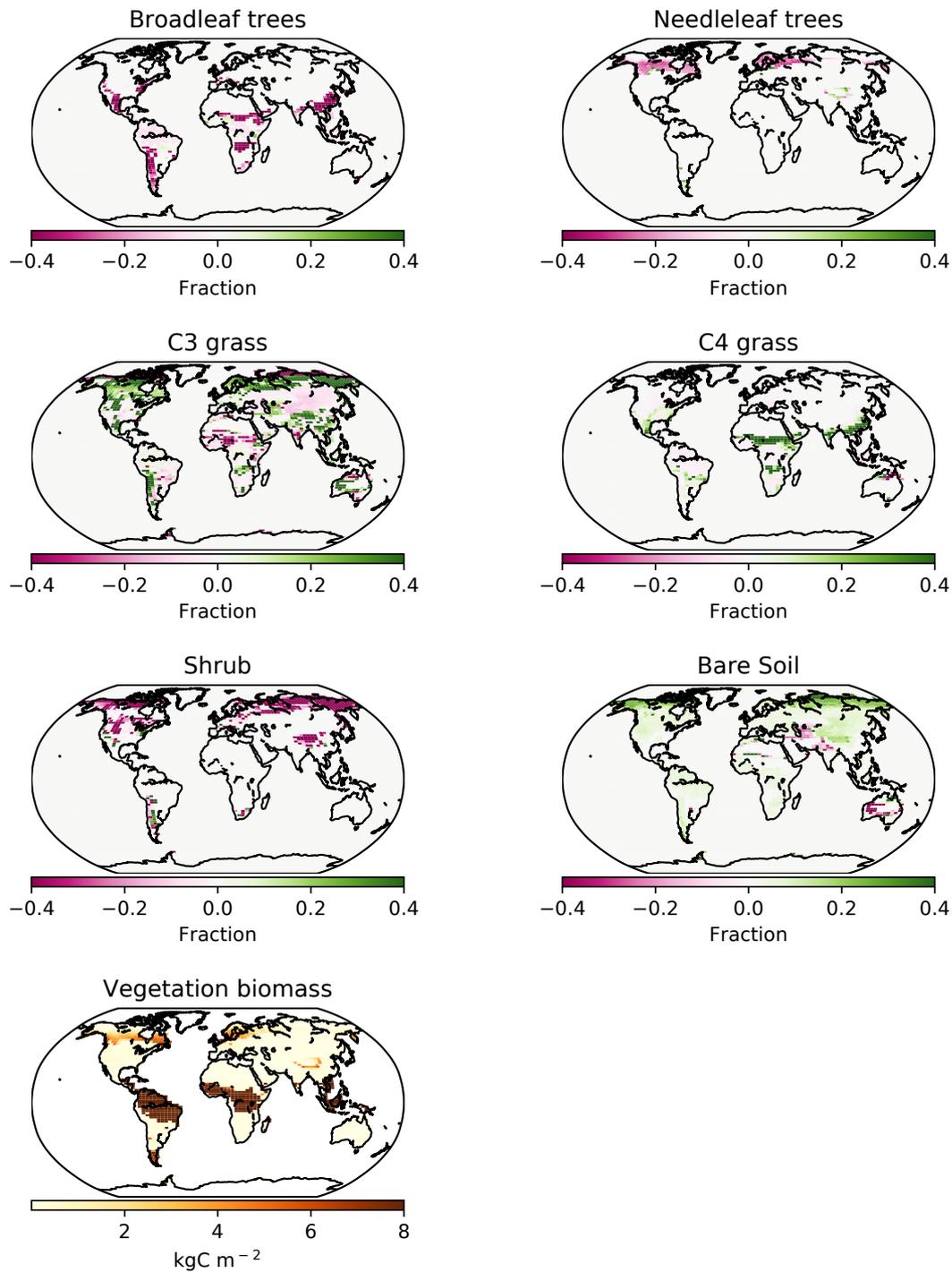
Figure 6. PFTs fractions in the UVic ESCM for 1980-2010, CNP minus baseline. Bottom last plot shows CNP global biomass distribution.
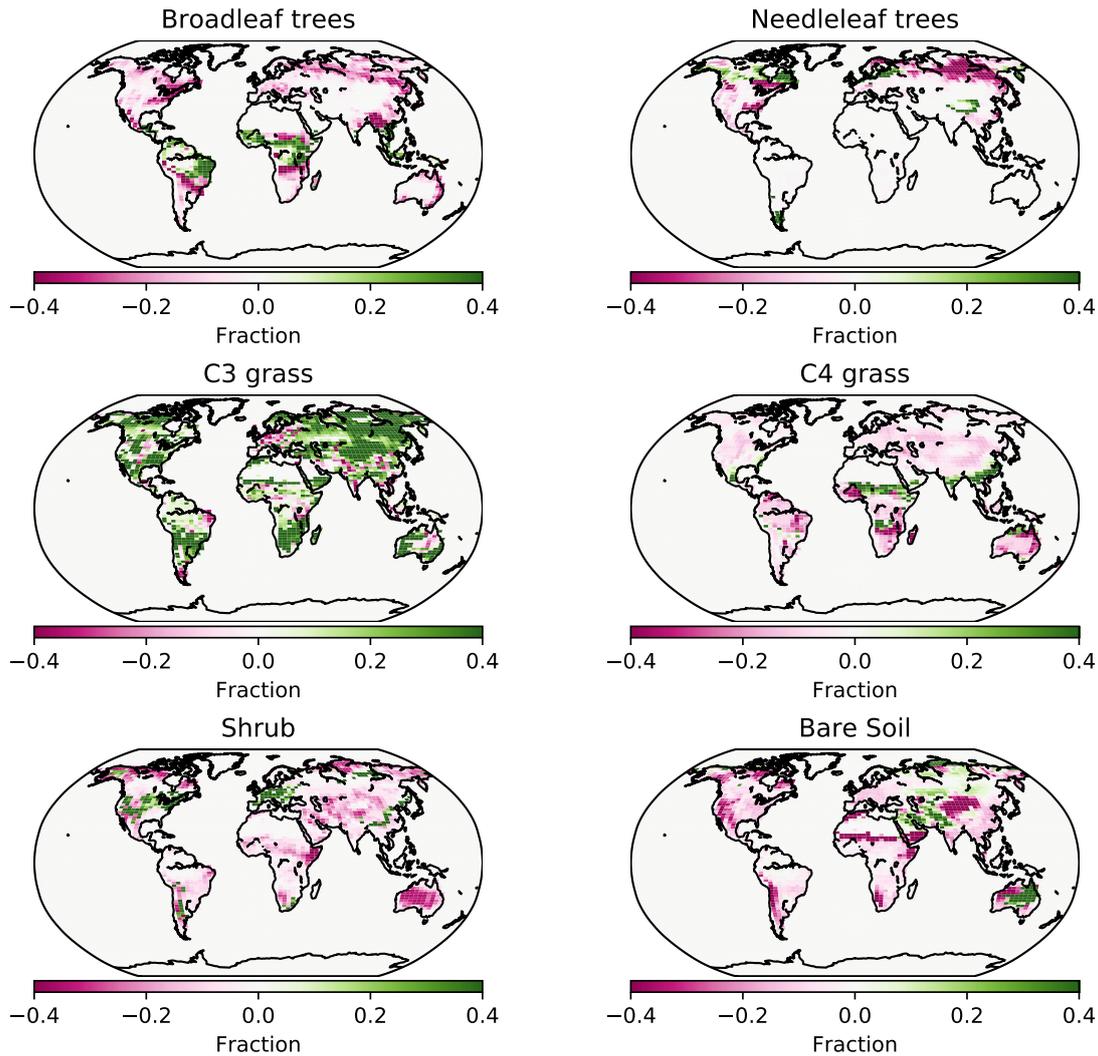
Figure 7. PFTs fractions in the UVic ESCM for 2008-2012, CNP minus Poulter et al. 2015 PFTs dataset.

The total vegetation carbon are similar to Wania et al. (2012), with tropical forest having a range from 8-16 kgC m^{-2} and

390   4-12 kgC m^{-2} in temperate and boreal forest with means of 10.50 and 6.7 kgC m^{-2} respectively compared to 12-16 kgC m^{-2}

and 4-12 kgC m^{-2} and means of 13.4 and 7.3 kgC m^{-2}. The latitudinal mean shows a decrease in the range of vegetation

carbon in tropical latitudes of 1-1.5 kgC m^{-2} and 0.4-0.8 kgC m^{-2} in northern template latitudes. These results indicate that

the main reduction of vegetation carbon is in the tropics, which agrees with the general N and P global pattern (Du et al. ,

2020). Consistent with Wania et al. (2012) the vegetation carbon outputs are similar to 12.1 kgC m^{-2} for tropical and 5.7–6.4

395   for temperate and boreal forests to Malhi et al. (1999).
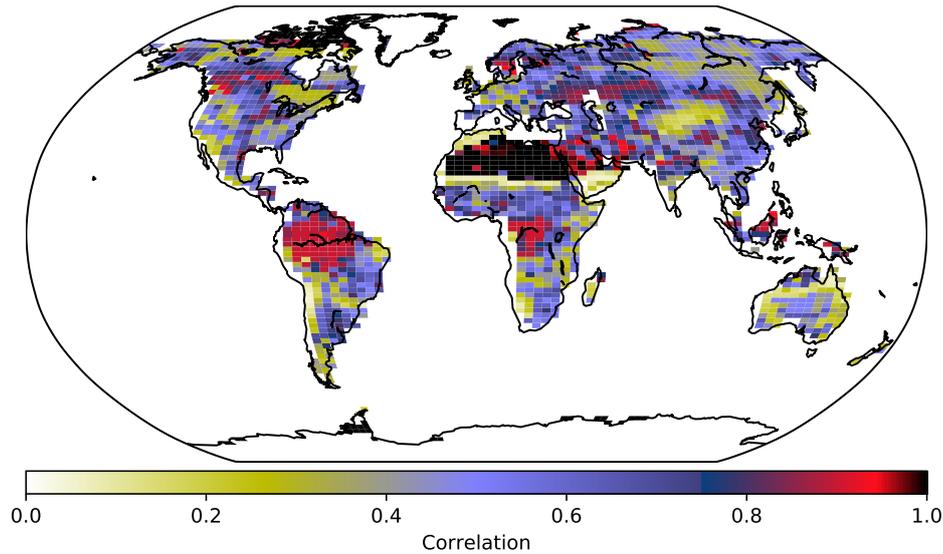
Figure 8. PFTs fractions across grid cells in the UVic ESCM for 2008-2012, CNP correlation to Poulter et al. (2015) PFTs dataset.

3.2 Nitrogen cycle

3.2.1 Nitrogen distribution

The soil ~~nitrogen~~ N ranges from 0 to 1.5~~kgC~~ kgN m^{-2} with lower N in tropics increasing towards the temperate regions. Globally, the CNP simulated soil ~~nitrogen~~ N is reduced compared to the original N structure in the UVic ESCM version 2.9 presented by Wania et al. (2012). The primary differences between Wania et al. (2012) N cycle and the current version are the soil layer structure and the stochiometry response to N limitation. In the former, N could be transfer from other pools when N was outside of the ratios threshold and thereby be considered to be limiting vegetation.

This result is also lower than the 0 to 4.8 ~~kgC~~ kgN m^{-2} from IGBP-DIS data base (Global Soil Data Task Group , 2000). Wania et al. (2012) stated that the N content in the model is depended to soil carbon fixed via a fixed CN ratio. Given this, lower carbon values can lower soil N values in CN simulations. Thereby, lower carbon in soil could be a strong reason why our results have less N than IGBP-DIS data base (Global Soil Data Task Group , 2000) and Wania et al. (2012). However, our values fall within the range of uncertainty. Our model estimates a mean ~~biological nitrogen fixation~~ BNF for 2010-2020 of 119 Tg N yr^{-1}. This value is above 35 Tg N yr^{-1} from Braghiere et al. (2022) and within the range of 52–130 Tg N yr^{-1} presented by Barnard and Friedlingstein (2020)

3.2.2 Vegetation nitrogen

The total amount of vegetation ~~nitrogen~~ N (2.20 Pg N) was lower than the previous N cycle (2.94 Pg N, Wania et al. (2012)). These values are similar to Zaehle et al. (2010) (3.8 Pg N) and Wang et al. (2018) (3.9 PgN) but lower than Li et al. (2000) (16Pg N) and Yang et al. (2009) (18 Pg N). Our tropical (30 to 45gN m^{-2}) and boreal forest vegetation ~~nitrogen~~ N (20 to 35gN m-2) results are lower than from Wania et al. (2012) (30 to 40gN m^{-2}), and those of Xu-ri and Prentice (2008) and Yang et al. (2009) (both studies ranged between of 150 to 400 gN m^{-2})

The global pattern of CN ratio is similar to Wania et al. (2012) structure with the highest located in tropical regions especially South America and South East Asia. Tropical forests show a value that ranges from 230-280 C:N (Figure 9) compared to 250-300 C:N to Wania et al. (2012). The reduction in wood carbon in tropics by P limitation in CNP lowered the C:N ratios. Our values are within the observational range of uncertainty (95-730) stated in Martius (1992).

The distribution of vegetation N resembles the results of Du et al. (2020) where N primary effect in higher latitudes. The PFTs fraction changes show that N mainly limits North and central America (BR and NL), Chile (BR), Argentinian Patagonia (BR), North Europe (NL) and East Asia (BR)(Fig. 6). However, there seems to be N limitation in the tropical Africa and Asia in our model simulations. Even though our model does not represent co-limitation the stochiometric limitation does seems to indirectly capture this effect.

3.2.3 N$_2$O fluxes

The multilayer model has allowed the estimations of anoxic regions and hence, a major improvement in the model is the quantification of terrestrial N$_2$O flux. Figure 10 shows CN and CNP N$_2$O fluxes from 1990 to 2018. Compared to EDGAR version 6 dataset (Crippa et al. , 2021) our model simulates N$_2$O fluxes relatively well, agreeing mostly in last 10 years of the values. However, we observed an overestimation from 1990 to 2010. The CN version of the model fit within the lower natural (Natural soil, Atmospheric N deposition on land) + anthropogenic (Agriculture, Fossil fuel and industry) emission range (8.9 -14.3 Tg N yr^{-1}) given by the global carbon project (Tian , 2020) while CNP fall just below the lower range value. The reduction of N in the model system by P effect is shown by this results, the reduction of vegetation biomass and then litterfall reduces the amount of N transfer to the N soil pool limiting the natural denitrification. The lack of oceanic production of N$_2$O in the model makes the comparison with the global total N$_2$O flux impossible at the moment. The total estimates for N$_2$O emissions being 4.2 to 11.4 Tg N yr^{-1} anthropogenic and 8.0 to 12.0 Tg N yr^{-1} natural given by global carbon project (Tian , 2020). Assuming an ocean output of a mid-range emission (3.4 Tg N yr^{-1}) the model simulations are close to the lower range of the emission reported with CN (13.3 Tg N yr^{-1}) and CNP (12.1 Tg N yr^{-1}). Lighting and atmospheric production, biomass burning (addition of N$_2$O to atmospheric pool) and post deforestation pulse effect are not taken into account in the model structure and that could improve the fit of the simulation to a mid-range level value.
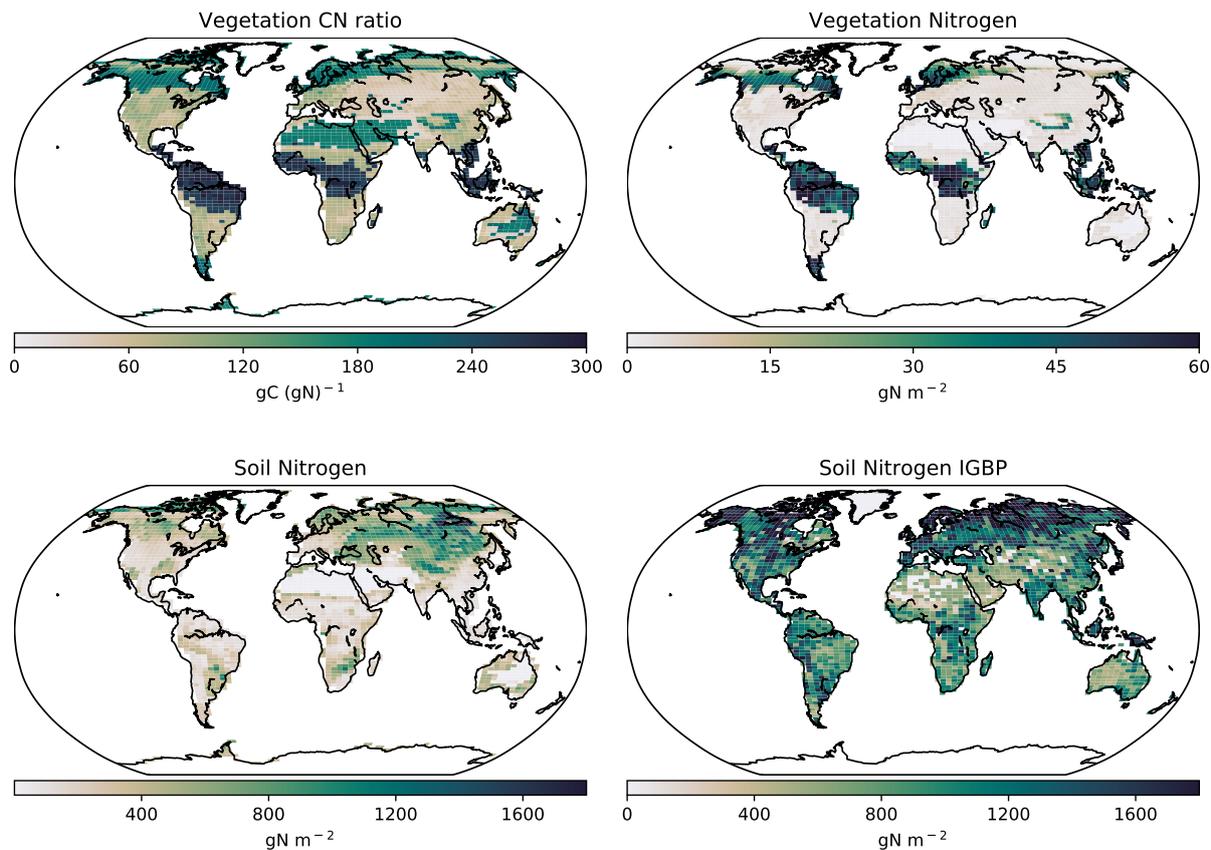
Figure 9. Modelled global soil and vegetation ~~nitrogen~~ N in the CNP version of the UVic ESCM from 1980-1999. Lower right map corresponds to the soil ~~nitrogen~~ N from the IGBP-DIS dataset (Global Soil Data Task Group , 2000)

3.3 Phosphorus cycle

3.3.1 Inputs and losses

The P global weathering rate estimated is 3 Tg P yr^{-1} similar to 2 Tg P yr^{-1} in Wang et al. (2010). Fertilization inputs of 1 Tg P yr^{-1} (Filipelli , 2002) where added as an option to the model but were not used for the current simulations and dust deposition is not accounted for. Hence, the only P input into the system in this experimental set-up comes from rock weathering. Regarding the P weathering representation Hartmann et al. (2014) approach was tested at first, but Wang et al. (2010) weathering scheme resulted in a better, simplified and controllable input. Although, Hartmann et al. (2014) was found
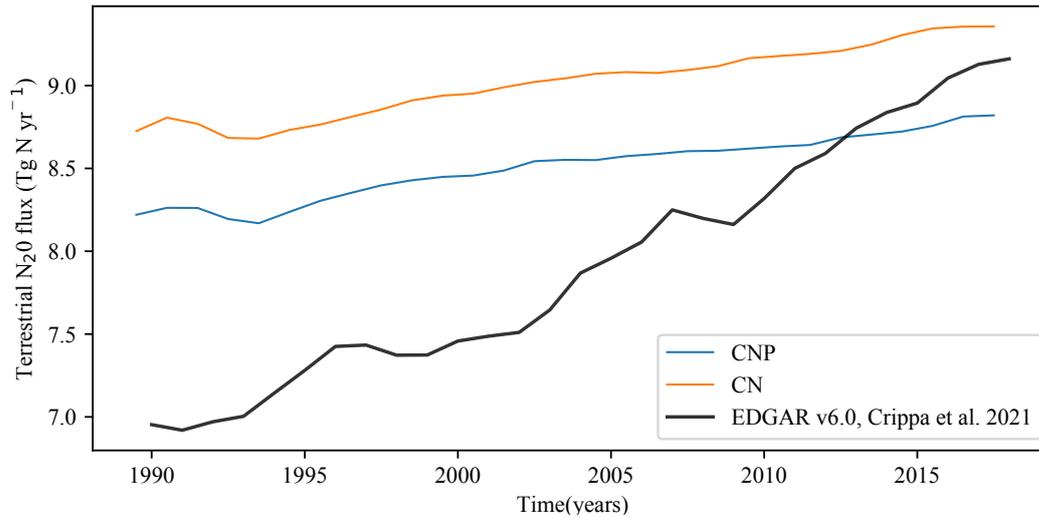
Figure 10. CNP and CN global soil N_2O emissions vs EDGAR version 6.0 N_2O dataset (Crippa et al. , 2021).

to be superior since P input is dynamic, incorporating model runoff and lithological map distribution. A dynamic P input will also require a better representation of P losses in order to maintain a steady state.

The P weathering was set so the loss by leaching (3 Tg P yr^{-1}) were in accordance with the rates of was comparable with to the riverine input stated in Filipelli (2002) of 4-6 Tg P yr^{-1}. The gap corresponds to anthropogenic inputs not included here, the pre-industrial ~~phosphorus~~ P input to the ocean from riverine input is 2-3 Tg P yr^{-1} and the human activities especially agriculture (fertilizers) and water wastes roughly correspond to a doubling of the P input.

3.3.2 Land P pools and storages

The total inorganic and organic P values are similar as those shown in the results of Smil (2000), Mackenzie (2002) and Wang et al. (2010) (Table 7), although organic P is slightly underestimated in the model (3.5 Pg P). This underestimation is likely the result of ~~a high mineralization rate~~the lack of P fertilization on land. The labile, sorbed, strongly sorbed P and occluded pools are comparable values to Wang et al. (2010).

Globally the total soil P distribution (Fig. 11) is comparable to the He et al. (2021) dataset, which is one of the few terrestrial ~~phosphorus~~ P concentrations maps available. Overall, the model simulates less global P especially in northern latitudes most likely due to the oversimplified weathering scheme that underestimated the inputs in higher latitudes.

Latitudinally, the tropical soils showed the lowest P with exception of highlands and mountains while increasing sequentially to the northern latitudes as showed in He et al. (2021). The labile P shows a similar distribution to Yang et al. (2013) with tropical regions being relatively depleted compared to other regions due to the high adsorption and occlusion by the soils.
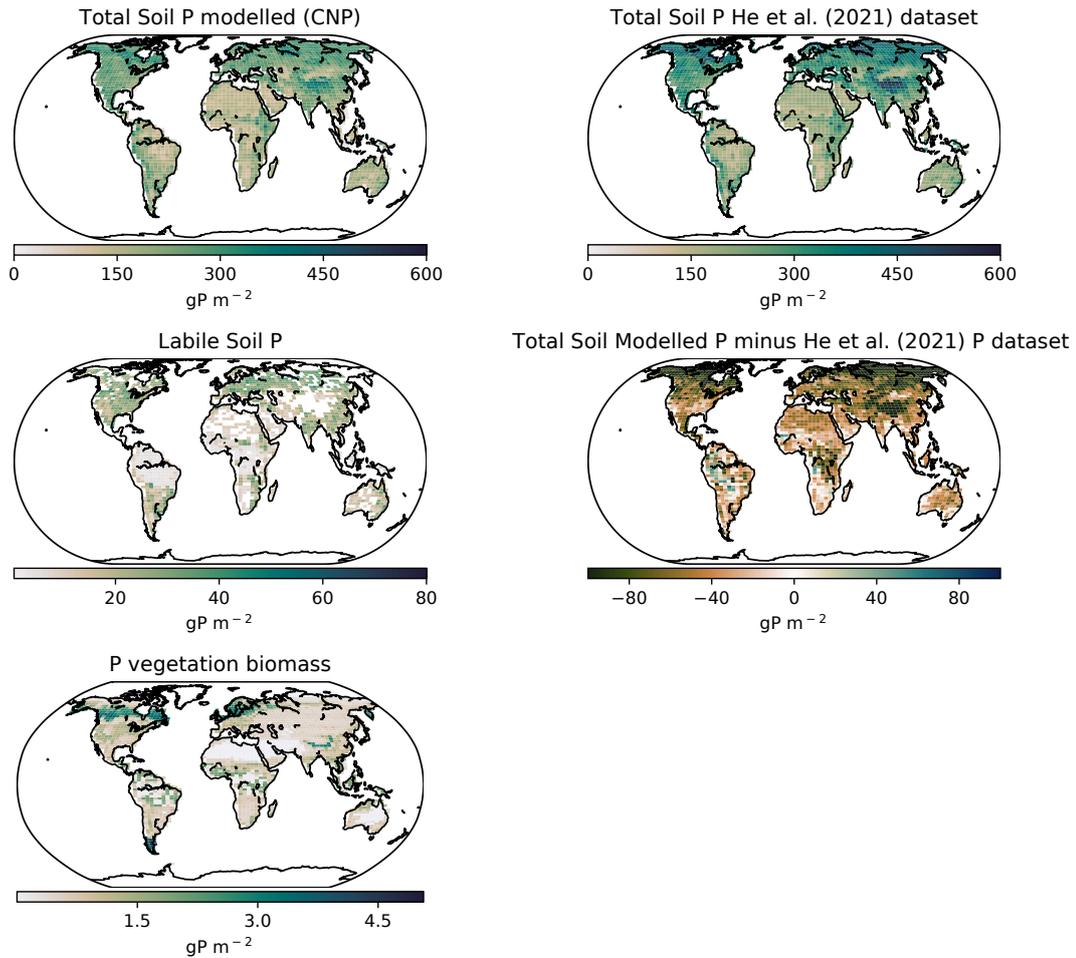
Figure 11. Soil and vegetation P global distribution. Modelled total P in soil, total P in soil as in He et al. 2021, soil P, labile P, vegetation biomass and the difference between modelled and observational P from He et al. (2021).

In contrast with N, ~~phosphorus~~ P inputs is limited by the mineral (apatite) concentration and weathering rate rather than biologically fixed. Most of the P is retain by soils leaving a small labile fraction for biological uptake. Because P mineral weathering and chemical recycling in the soils are so constraining, our linear model approach for adsorption based on Goll et al. (2017) might overestimate the impact of adsorption and occlusion in tropical soils. It is also worth noting that the biological impact on the adsorption-desorption dynamics is missing in most P modules in ESMs. The release of P from mineral grains can be enhanced by either the reduction of pH due to respiration, the direct addition of organic acids by plants roots Schlesinger (1997).

3.3.3 Phosphorus in vegetation

The terrestrial vegetation shows a slight underestimation in comparison with other models. The new stochiometry limitation scheme of the model plays an important role in the vegetation biomass and could be the reason for the underestimated values specially for tropical regions. However, the range of P in terrestrial vegetation is still uncertain with several studies showing a range from 1.8-3.0 Pg P (Smil , 2000). Although Wang et al. (2010) have dismissed those values as overestimations given an overall N:P ratio of 10-20 gN gP $^{-1}$, 3 Pg P is simply too high to be met.

Table 7. Phosphorus cycle model pools and values for literature.

Variables	Value (Pg P)	References (Pg P)
Total inorganic P	20.8	35-40 Smil (2000)
Total organic P	3.5	36 Mackenzie (2002)
		26.5 Wang et al. (2010)
		13.7 Wang et al. (2018)
		5-10 Smil (2000)
Labile P	1.4	5 Mackenzie (2002)
		5.7 Wang et al. (2010)
		8.6 Yang et al. (2013)
		1.5 Wang et al. (2010)
Sorbed P	1.1	3.6 Yang et al. (2013)
		1.7 Wang et al. (2010)
Strongly sorbed P	12	7.6 Wang et al. (2010)
Occluded	6.3	9.0 Wang et al. (2010)
Vegetation P	0.2	0.4 Wang et al. (2010)
		0.5 Smil (2000)
		0.5 Wang et al. (2018)
		0.2 Wang et al. (2018)
P Litter	0.01	0.5 Mackenzie (2002)
		0.04 Wang et al. (2010)
		0.03 Wang et al. (2018)

The foliar stochiometry seems to approximately follow the N:P ratio field measurements of Reich and Oleksyn (2004) (Fig. 12). The tropical regions show some underestimated values in our model, the low amount of labile P and the latter decrease in broadleafs trees biomass could be responsible for the low numbers. Similarly, Nakhavali et al. (2021) show model values of 4-15 gP m^{-2} for an Amazonian site which surpasses our results.
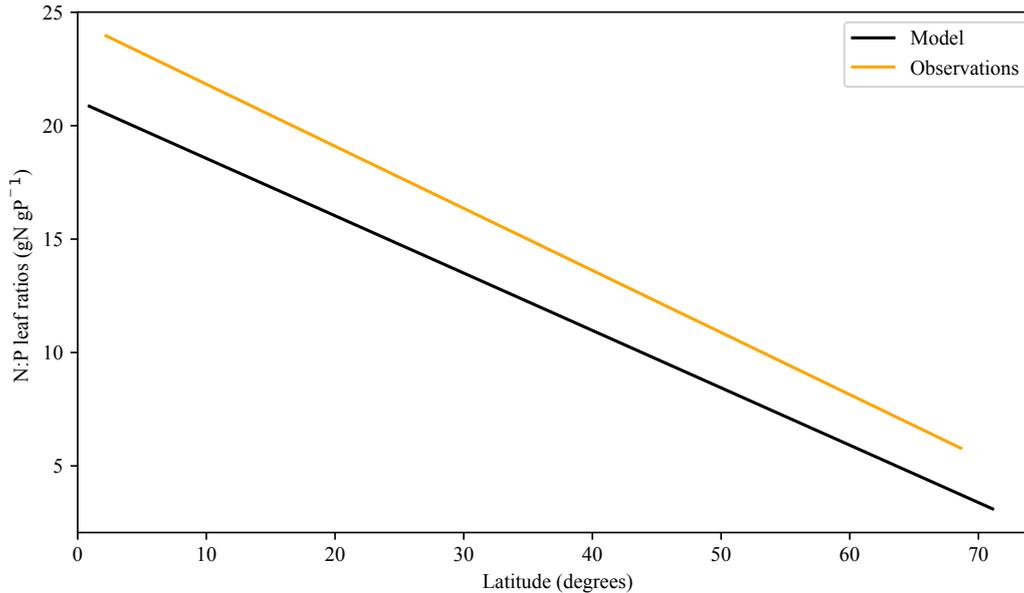
Figure 12. Modelled N:P leaf ratios trend vs an empirical relationship derived from Reich and Oleksyn (2004).

A more complex adsorption – desorption scheme might be beneficial to solve the underestimation for tropical latitudes as those regions are heavily sorbed and loose most of the input P, even though, the need of a proper global P vegetation dataset is imperative to have proper ranges in global distributions. The mechanical reduction of vegetation stochiometrically by the model structure might also be too simplistic to represent P limitation in tropics.

3.4 Parameter sensitivity

485

We perturbed 6 parameters (CP$_{leafmax}$, CN$_{leafmax}$, R$_{leafp}$, R$_{leafn}$, V$_{maxp}$, V$_{maxn}$) over historical simulations to assess the model sensitivity in terms of limitation of N and P. All of the above parameters play an important role in the nutrient limitation structure of the model. P$_{leafmax}$, N$_{leafmax}$ control when the stochiometrical limitation is set to be enforced on terrestrial vegetation and R$_{leafp}$, R$_{leafp}$, V$_{maxp}$ and V$_{maxn}$ control the uptake, litterfall and allocation of nutrients in leafs. In each
490 case, default values were increased and decreased by 10% and 20% while holding other parameters constant. The results were compared to model simulations with all parameters held constant and set to default values. The cumulative atmosphere-land carbon flux was used to measure the effect of the perturbation, since the limitation directly affects this flux.

The results of the sensitivity study show that model sensitivity varies with different parameters (Table 8). The UVic ESCM is most sensitive to perturbations of CP$_{leafmax}$ and CN$_{leafmax}$ because both determine directly the threshold by which vegetation
495 carbon is reduced and nutrient limitation is defined. The model seems to be most sensitive to changes in CP$_{leafmax}$. The

regulation of this parameter is very useful to calibrate woody vegetation in tropical regions to improve the cover representation. The other parameters have a lower impact on the atmosphere-land carbon flux ranging from -3.23% to +1.60%.

Table 8. Cumulative atmosphere-land carbon flux anomaly from baseline (%). The parameters were perturbed by increasing and reducing 10 and 20 % of their value.

Parameters	-20%	-10%	+10%	+20%
$CP_{leafmax}$	-16.04%	-3.03%	+0.25%	+0.26%
$CN_{leafmax}$	-6.46 %	-2.10 %	+8.63%	+12.58%
R_{leafp}	-0.23%	-0.12%	+0.22%	+0.26%
R_{leafn}	-0.98%	-0.76%	+1.20%	+1.60%
V_{maxp}	-3.23%	-0.94%	+0.18%	+0.22%
V_{maxn}	-1.30%	-1.10%	+0.95%	+1.45%

4   Limitations and applications of the terrestrial nutrient modules

The UVic ESCM has been a critical tool in developing the cumulative emissions framework to climate mitigation (Zickfeld et al. , 2009; Matthews et al. , 2009; Matthews and Weaver , 2009; MacDougall and Knutti , 2016; Mengis et al. , 2018; Tokarska et al. , 2019) due to its low computations cost and strict enforcement of matter and energy conservation the model is capable of conducting a host of simulation beyond the limits of most other models, but with higher resolution than other EMICs (e.g. Montenegro et al. (2007); Matthews and Caldeira (2008); Keller et al. (2014); MacDougall and Knutti (2016); MacDougall (2017); Pahlow et al. (2020); Kvale et al. (2021)) . As terrestrial nutrient limitation constrains the carbon cycle in nature, the new ~~nitrogen and phosphorus~~ N and P modules allows addressing research questions relating carbon budgets, carbon cycle and CH_4 feedbacks, carbon dioxide removal and permafrost carbon cycle, among other questions. Furthermore, the ~~nitrogen and phosphorus~~ N and P cycles can represent environmental and climate critical processes such as the release of N_2O, agricultural impacts on terrestrial soils and coastal lines, eutrophication, anoxic events and nutrient fluxes from land to ocean.

A number of limitations have been identified with the developed N and P modules that relate to the degree of complexity or the lack of large-scale datasets available. Due to the lack of global estimates of nutrient pools and fluxes based on field measurements, many of the parameters or parameterizations in this model are poorly constrained. In general, these are the following model ~~limitations that should be addressed in further studies~~ limitation that are plan to be improved in future model development projects:

1. The model does not include a dynamic nutrient leaf resorption rate. Under nutrient limitations, this rate can increase as a strategy to conserve nutrients (Reed et al. , 2012). Thus, the effect of limitation in our model might be overestimated.

2. There is a static input of P from weathering. To control the P input we chose to estimate weathering flux by adding a fix amount. This oversimplification could add more uncertainty to the P pools and can be overcome using a runoff based weathering scheme. Moreover, we do not account for P atmospheric dust deposition.

3. The sorption-desorption dynamics of P in soil are oversimplified. We chose Goll et al. (2017) approach because it was a simpler way to represent this process. However, a more complex solution might improve the distribution P globally.

4. The absence of an ocean N_2O output. Consequently, we are unable to estimate the total amount of a dynamically evolving N_2O concentration at this time. As N_2O is the 3rd most important greenhouse gas (IPCC , 2022), its incorporation into the model is a priority.

5. The model does not account for root uptake constrains of N and P on terrestrial vegetation. This includes spatial representations of mycorrhizal associations and the carbon cost of nitrogen and phosphorus uptake from soil (Shi et al. , 2016; Braghiere et al. , 2021, 2022).

The CNP model is primarily designed to improve carbon cycle feedbacks under current and future climate conditions. The use of nutrient limitation improves the land-atmosphere dynamics. In simulations, this improvement has a significant impact on atmospheric CO_2 concentrations. In future studies, we intend to assess the impact of nutrient limitation on different SSP scenarios and key carbon cycle benchmark metrics. Furthermore, the model can be used to improve the vegetation representation in ESMs. Finally, the CNP model may be used to generate coastal nutrient input and to integrate terrestrial nutrient biogeochemical processes with oceanic processes.

5   Conclusion

The N and P cycles simulated here fit the range of uncertainty shown in data-sets and other modelling efforts. Generally, our values fall into the lower range of the spectrum. N limits mainly high latitudes especially in northern regions, but do shows some limitation in tropical Africa and Asia. P limitations is greater in tropical regions and reduced the vegetation biomass compared to the carbon only version of the model bringing the model closer in line with observation (Mengis et al. (2020)).

The two nutrient limitation have improved the representation of the atmospheric carbon concentration in simulations forced with CO_2 emissions, using the Keeling curve as benchmark data. The land-atmospheric flux fits other simulations datasets and have been reduced from Mengis et al. (2020) values. Overall N and P addition have improved the carbon cycle feedbacks simulated in historical simulations. The GPP is lowered especially in tropics mainly due to the reduction of woody vegetation biomass.

Many improvements remain to be made in our model structure. In regards with N cycle denitrification processes need to be improved, N_2O fluxes while in the same magnitude as observations lack the trend showed in other benchmark datasets. The complexity of the P cycle could be improved especially the input and sorption processes. Finally both N and P cycles could gain accuracy from adding dynamics leaf re-absorption rates that has been shown to change when nutrient limitation is present in the ecosystem and that can be used as in Du et al. (2020) to clearly map the limitation pattern. Despite these limitations the improved model has shown higher fidelity to observations and is expected to improve projections of the future of key carbon cycle feedbacks.

Code and data availability.

The model code and data used for this paper are available at:
https://borealisdata.ca/dataset.xhtml?persistentId=doi:10.5683/SP3/GXYZKU.

Author contributions.

AHMD initiated the redevelopment of the N module. MD ported the N module to the UVic ESCM version 2.10 and further improved it. MD developed the ~~phosphorus~~ P cycle. MD wrote the paper and AHMD provided supervisory support. NM contributed with the interpretation and validation of the model results. SA contributed with the visual representation of the ~~phosphorus~~ P module structure and model results.

Competing interests.

The authors declare that they have no conflict of interest.

560 *Acknowledgements.* AHMD and MD are grateful for support from the Natural Science and Engineering Research Council of Canada Discovery Grant program and support from Compute Canada (now the Digital Research Alliance of Canada). We are indebted to M. Eby for early advise on implementing the Nitrogen ~~verion~~ version of the model and for providing the model code for the original N cycle verion of UVic ESCM.

References

Archer, D.: A data-driven model of the global calcite lysocline, Global Biogeochem. Cy., 10, 511–526, https://doi.org/10.1029/96GB01521, 1996.

Arora, V. K., Katavouta, A., Williams, R. G., Jones, C. D., Brovkin, V., Friedlingstein, P., Schwinger, J., Bopp, L., Boucher, O., Cadule, P., Chamberlain, M. A., Christian, J. R., Delire, C., Fisher, R. A., Hajima, T., Ilyina, T., Joetzjer, E., Kawamiya, M., Koven, C. D., Krasting, J. P., Law, R. M., Lawrence, D. M., Lenton, A., Lindsay, K., Pongratz, J., Raddatz, T., Séférian, R., Tachiiri, K., Tjiputra, J. F., Wiltshire, A., Wu, T. and Ziehn, T.: Carbon-concentration and carbon-climate feedbacks in CMIP6 models and their comparison to CMIP5 models, Biogeosciences, 17, 4173–4222, doi:10.5194/bg-17-4173-2020, 2020.

Avis, C. A.: Simulating the Present-Day and Future Distribution of Permafrost in the UVic Earth System Climate Model, PhD thesis, University of Victoria, 2012.

Davies-Barnard, T., and Friedlingstein, P. The global distribution of biological nitrogen fixation in terrestrial natural ecosystems. Global Biogeochemical Cycles, 34. 2020. e2019GB006387. https://doi.org/10.1029/2019GB006387

Braghiere, R. K., Fisher, J. B., Fisher, R. A., Shi, M., Steidinger, B. S., Sulman, B. N., et al. Mycorrhizal distributions impact global patterns of carbon and nutrient cycling. Geophysical Research Letters, 48, e2021GL094514. https://doi.org/10.1029/2021GL094514. 2021.

Braghiere, R. K., Fisher, J. B., Allen, K., Brzostek, E., Shi, M., Yang, X., et al. Modeling global carbon costs of plant nitrogen and phosphorus acquisition. Journal of Advances in Modeling Earth Systems, 14. 2022. e2022MS003204. https://doi.org/10.1029/2022MS003204

Bonan, G. B. and Levis, S.: Quantifying carbon-nitrogen feedbacks in the Community Land Model (CLM4), Geophys. Res. Lett., 37, 2261–2282, 2010.

Bitz, C. M., Holland, M. M., Weaver, A. J., and Eby, M.: Simulating the ice-thickness distribution in a coupled, J. Geophys. Res., 106, 2441–2463, https://doi.org/10.1029/1999JC000113, 2001.

Chen, Xiaodong Dunfield, K. Fraser, Tandra D Wakelin, Steven Richardson, A. Condron, L.M.. (2019). Soil biodiversity and biogeochemical function in managed ecosystems. Soil Research. 58. 10.1071/SR19067.

Clark, D. B., Mercado, L. M., Sitch, S., Jones, C. D., Gedney, N., Best, M. J., Pryor, M., Rooney, G. G., Essery, R. L. H., Blyth, E., Boucher, O., Harding, R. J., Huntingford, C., and Cox, P. M.: The Joint UK Land Environment Simulator (JULES), model description – Part 2: Carbon fluxes and vegetation dynamics, Geosci. Model Dev., 4, 701–722, https://doi.org/10.5194/gmd-4-701-2011, 2011.

Cox, P., Huntingford, C., Harding, J. A canopy conductance and photosynthesis model for use in a GCM land surface scheme. Journal of Hydrology, Volumes 212–213. 1998. https://doi.org/10.1016/S0022-1694(98)00203-0.

Cox, P. M., Betts, R. A., Bunton, C. B., Essery, R. L. H., Rowntree, P. R., and Smith, J.: The impact of new land surface physics on the GCM simulation of climate and climate sensitivity, Clim. Dynam., 15, 183–203, 1999.

Cox, P. M.: Description of the TRIFFID dynamic global vegetation model, Tech. Rep. 24, Hadley Centre, Met office, London Road, Bracknell, Berks, RG122SY, UK, 2001.

Collier, N., Hoffman, F. M., Lawrence, D. M., Keppel-Aleks, G., Koven, C. D., Riley, W. J., Mu, M. and Randerson, J. T.: The International Land Model Benchmarking (ILAMB) System: Design, Theory, and Implementation, J. Adv. Model. Earth Syst., 10(11), 2731–2754, doi:10.1029/2018MS001354, 2018.

Cotrufo, M.F., Wallenstein, M.D., Boot, C.M., Denef, K. and Paul, E. The Microbial Efficiency-Matrix Stabilization (MEMS) framework integrates plant litter decomposition with soil organic matter stabilization: do labile plant inputs form stable soil organic matter?. Glob Change Biol, 19: 988-995. https://doi.org/10.1111/gcb.12113. 2013.

Crippa, M., Guizzardi, D., Muntean, M., Schaaf, E., Lo Vullo, E., Solazzo, E., Monforti-Ferrario, F., Olivier, J. and Vignati, E.: EDGAR v6.0 Greenhouse Gas Emissions. European Commission, Joint Research Centre (JRC). 2021. [Dataset] PID: http://data.europa.eu/89h/97a67d67-c62e-4826-b873-9d972c4f670b.

Cross, A. F and Schlesinger, W. H.: A literature review and evaluation of the Hedley fractionation: applications to the biogeochemical cycle of soil phosphorus in natural ecosystems, Geoderma,64, 197–214, 1995.

Davidson, E.,Keller, M, Erickson, H., Verchot, L. and Veldkamp, E.: Testing a conceptual model of soil emissions of nitrous and nitric oxides: using two functions based on soil nitrogen availability and soil water content, the hole-in-the-pipe model characterizes a large fraction of the observed variation of nitric oxide and nitrous oxide emissions from soils. AIBS Bulletin, 50 (8), 667–680, 2000.

Dynarski, K. A., Morford, S. L., Mitchell, S. A., Houlton, B. Z. Bedrock nitrogen weathering stimulates biological nitrogen fixation. Ecology, 100(8), 1–10. 2019. https://www.jstor.org/stable/26749507.

Du, E., Terrer, C., Pellegrini, A., Ahlstrom, A., Van Lissa, C., Zhao, X., Xia, N., Wu, X. and Jackson, R.: Global patterns of terrestrial nitrogen and phosphorus limitation, Nat. Geosci. 13, 221–226, https://doi.org/10.1038/s41561-019-0530-4, 2020.

Eisele, K., Schimel, D., Kapustka, L., Parton, W.: Effects of available P and N:P ratios on non-symbioticdinitrogen fixation in tall grass prairie soils. Oecologia 79, 471–474, 1989.

Fleischer, K., Dolman, A. J., van der Molen, M. K., Rebel, K. T., Erisman, J. W., Wassen, M. J., et al. (2019). Nitrogen deposition maintains a positive effect on terrestrial carbon sequestration in the 21st century despite growing phosphorus limitation at regional scales. Global Biogeochemical Cycles, 33, 810– 824. https://doi.org/10.1029/2018GB005952

Filippelli, G.: The global phosphorus cycle, in phosphates: Geochemical, geobiological, and materials importance, Reviews in Mineralogy and Geochemistry, 391-425. 2002.

Firestone, M. and Davidson, E.: Microbiological basis of NO and N2O production and consumption in soil. Exchange of trace gases between terrestrial ecosystems and the atmosphere, 47, 7–21, 1989.

Fisher, J., Badgley, G. and Blyth, E.: Global nutrient limitation in terrestrial vegetation, Global Biogeochemical Cycles 6, https://doi.org/10.1029/2011GB004252, 2012.

Fowler, D., Coyle, M., Skiba, U., Sutton, M. A., Cape, J. N., Reis, S., Sheppard, L. J., Jenkins, A., Grizzetti, B., Galloway, J. N., Vitousek, P., Leach, A., Bouwman, A. F., Butterbach-Bahl, K., Dentener, F., Stevenson, D., Amann, M., Voss, M. The global nitrogen cycle in the twenty-first century. Philosophical transactions of the Royal Society of London. Series B, Biological sciences, 368(1621), 2013. https://doi.org/10.1098/rstb.2013.0164

Gedney, N. and Cox, P.: The sensitivity of global climate model simulations to the represen- tation of soil moisture heterogeneity. Journal of Hydrometeorology, 4 (6), 1265–1275, 2003.

Gerber, S., Hedin, L. O., Oppenheimer, M., Pacala, S. W., and Shevliakova, E.: Nitrogen cycling and feedbacks in a global dynamic land model, Global Biogeochem. Cy., 24, 121–149, 2010.

Global Soil Data Task Group: Global gridded surfaces of selected soil characteristics (IGBP-DIS), Oak Ridge National Laboratory Distributed Active Archive Center, Oak Ridge, Tennessee, U.S.A., http://www.daac.ornl.gov, 2000.

Global Soil Data Task.:Global Soil Data Products CD-ROM Contents (IGBP-DIS). Data Set. Available online [http://daac.ornl.gov] from Oak Ridge National Laboratory Distributed Active Archive Center, Oak Ridge, Tennessee, U.S.A. http://dx.doi.org/10.3334/ORNLDAAC/565. 2014.

Goll, D., Brovkin, V., Parida, B., Reick, C., Kattge, J., Reich, P., van Bodegom, P., and Niinemets, Ü.: Nutrient limitation reduces land carbon uptake in simulations with a model of combined carbon, nitrogen and phosphorus cycling, Biogeosciences 9, 3547–3569, https://doi.org/10.5194/bg-9-3547-2012, 2012.

640 Goll, D., Vuichard, N., Maignan, F., Jornet-Puig, A., Sardans, J., Violette, A., Peng, S., Sun, Y., Kvakic, M., Guimberteau, M., Guenet, B., Zaehle, S., Penuelas, J., Janssens, I. and Ciais, P.: A representation of the phosphorus cycle for ORCHIDEE. Geoscientific Model Development 10, 3745-3770, doi.org/10.5194/gmd-10-3745-2017, 2017.

Haverd, V., Smith, B., Nieradzik, L., Briggs, P. R., Woodgate, W., Trudinger, C. M., Canadell, J. G., and Cuntz, M.: A new version of the CABLE land surface model (Subversion revision r4601) incorporating land use and land cover change, woody vegetation
645 demography, and a novel optimisation-based approach to plant coordination of photosynthesis, Geosci. Model Dev., 11, 2995–3026, https://doi.org/10.5194/gmd-11-2995-2018, 2018.

He, X., Augusto, L., Goll, D., Ringeval, B., Wang, Y., Helfenstein, J., Huang, Y., Yu, K., Wang, Z., Yang, Y. and Hou, E.: Global patterns and drivers of soil total phosphorus concentration, Earth System Science Data 13, 5831-5846, doi.org/10.5194/essd-13-5831-2021, 2021.

Hartmann, J. and Moosdorf, N.: The new global lithological map database GLiM: a representation of rock properties at the Earth surface,
650 Geochem. Geophy. Geosy. 13, 1–37, https://doi.org/10.1029/2012GC004370, 2012.

Hartmann, J., Moosdorf, N., Lauerwald, R., Hinderer, M.,and West, A.:Global chemical weathering and associated P-release - The role of lithology, temperature and soil properties, Chem.Geol. 363, 145–163, https://doi.org/10.1016/j.chemgeo.2013.10.025, 2014.

Hedley, M. and Stewart, J.: Method to measure microbial phosphate in soils, Soil Biol. Biochem. 14, 377–385, 1982.

Hungate, B., Dukes, J., Shaw, M, Luo, Y. and Field, C.: Nitrogen and Climate Change, Science (New York, N.Y.). 302, 1512-3,
655 10.1126/science.1091390, 2003.

IPCC, 2022: Climate Change 2022: Impacts, Adaptation, and Vulnerability. Contribution of Working Group II to the Sixth Assessment Report of the Intergovernmental Panel on Climate Change [H.-O. Pörtner, D.C. Roberts, M. Tignor, E.S. Poloczanska, K. Mintenbeck, A. Alegría, M. Craig, S. Langsdorf, S. Löschke, V. Möller, A. Okem, B. Rama (eds.)]. Cambridge University Press. In Press.

Jung, M., Koirala, S., Weber, U., Ichii, K., Gans, F., CampsValls, G., Papale, D., Schwalm, C., Tramontana, G., and Reichstein, M.: The
660 FLUXCOM ensemble of global landatmosphere energy fluxes, Scientific Data, in press, 6, https://doi.org/10.1038/s41597-019-0076-8, 2019.

Keller, D. P., Feng, E. Y., and Oschlies, A.: Potential climate engineering effectiveness and side effects during a high carbon dioxide-emission scenario, Nat. Commun., 5, 1–11, https://doi.org/10.1038/ncomms4304, 2014.

Kvale, K., Prowe, A.E.F., Chien, CT. et al. Zooplankton grazing of microplastic can accelerate global loss of ocean oxygen. Nat Commun
665 12, 2358 (2021). https://doi.org/10.1038/s41467-021-22554-w

Lampitt, R. and Achterberg, E., Anderson, R., Hughes, J., Iglesias, M., Kelly, B., Lucas, M., Popova, E., Sanders, R., Shepherd, J., Smythe, D. and Yool, A.: Ocean fertilization: a potential meansof geoengineering?, Philosophical Transactions of the Royal Society A: Mathematical, Physical and Engineering Sciences 366, 3919-3945, doi.org/10.1098/rsta.2008.0139, 2008.

Lawrence, D. M., Fisher, R. A., Koven, C. D., Oleson, K. W., Swenson, S. C., Bonan, G., et al. The Community Land Model version
670 5: Description of new features, benchmarking, and impact of forcing uncertainty. Journal of Advances in Modeling Earth Systems, 11, 4245– 4287. https://doi.org/10.1029/2018MS001583. 2019.

Le Quéré, C., Andrew, R. M., Friedlingstein, P., Sitch, S., Hauck, J., Pongratz, J., Pickers, P. A., Korsbakken, J. I., Peters, G. P., Canadell, J. G., Arneth, A., Arora, V. K., Barbero, L., Bastos, A., Bopp, L., Chevallier, F., Chini, L. P., Ciais, P., Doney, S. C., Gkritzalis, T., Goll, D. S., Harris, I., Haverd, V., Hoffman, F. M., Hoppema, M., Houghton, R. A., Hurtt, G., Ilyina, T., Jain, A. K., Johannessen, T., Jones,

675   C. D., Kato, E., Keeling, R. F., Goldewijk, K. K., Landschützer, P., Lefèvre, N., Lienert, S., Liu, Z., Lombardozzi, D., Metzl, N., Munro, D. R., Nabel, J. E. M. S., Nakaoka, S., Neill, C., Olsen, A., Ono, T., Patra, P., Peregon, A., Peters, W., Peylin, P., Pfeil, B., Pierrot, D., Poulter, B., Rehder, G., Resplandy, L., Robertson, E., Rocher, M., Rödenbeck, C., Schuster, U., Schwinger, J., Séférian, R., Skjelvan, I., Steinhoff, T., Sutton, A., Tans, P. P., Tian, H., Tilbrook, B., Tubiello, F. N., van der Laan-Luijkx, I. T., van der Werf, G. R., Viovy, N., Walker, A. P., Wiltshire, A. J., Wright, R., Zaehle, S., and Zheng, B.: Global Carbon Budget 2018, Earth Syst. Sci. Data, 10, 2141–2194,

680   https://doi.org/10.5194/essd-10-2141-2018, 2018.

Li, C.,Aber, J., Stange, F., Butterbach-Bahl, K. and Papen, H.: A process-oriented model of N2O and NO emissions from forest soils: 1. model development. Journal of Geophysical Research: Atmospheres, 105 (D4), 4369–4384, 2000.

Li, S., Lü, S., Liu, Y. et al. Variations and trends of terrestrial NPP and its relation to climate change in the 10 CMIP5 models. J Earth Syst Sci 124, 395–403. https://doi.org/10.1007/s12040-015-0545-1. 2015.

685   MacDougall, A.H. The oceanic origin of path-independent carbon budgets. Sci Rep 7, 10373. 2017. https://doi.org/10.1038/s41598-017-10557-x

MacDougall, A. H. and Knutti, R.: Projecting the release of carbon from permafrost soils using a perturbed parameter ensemble modelling approach, Biogeosciences, 13, 2123–2136, https://doi.org/10.5194/bg-13-2123-2016, 2016.

MacDougall, A. H., Avis, C. A., and Weaver, A. J.: Significant contribution to climate warming from the permafrost carbon feedback, Nat.
690   Geosci., 5, 719–721, 2012.

McGill, W., Cole, C.: Comparative aspects of cycling of organic C, N, S, and P through soil organic matter.Geoderma 26, 267–286, 1981.

Machado, C., Furlani, A.: KINETICS OF PHOSPHORUS UPTAKE AND ROOT MORPHOLOGY OF LOCAL AND IMPROVED VARIETIES OF MAIZE, Sci. Agric. (Piracicaba, Braz.), 61, 69-76, 2004.

Mackenzie, F., Ver, L. M., and Lerman, A.: Century-scale ni-trogen and phosphorus controls of the carbon cycle, ChemicalGeology, 190,
695   13–32, 2002.

Malhi, Y., Baldocchi, D. D., and Jarvis, P. G.: The carbon balance of tropical, temperate and boreal forests, Plant Cell Environ., 22, 715–740, 1999.

Martius, C.: Density, humidity, and nitrogen content of dominant wood species of floodplain forests (varzea) in Amazonia, Holz Roh Werkst., 50, 300–303, 1992.

700   Matthews, H., Gillett, N., Stott, P. et al. The proportionality of global warming to cumulative carbon emissions. Nature 459, 829–832. 2009. https://doi.org/10.1038/nature08047

Matthews, H., Weaver, A. Committed climate warming. Nature Geosci 3, 142–143. 2010. https://doi.org/10.1038/ngeo813

Matthews, H., and Caldeira, K. Stabilizing climate requires near-zero emissions, Geophys. Res. Lett., 35. 2008. doi:10.1029/2007GL032388.

Meissner, K. J., Weaver, A. J., Matthews, H. D., and Cox, P. M.: The role of land surface dynamics in glacial inception: a study with the
705   UVic Earth System Model, Clim. Dynam., 21, 515–537, https://doi.org/10.1007/s00382-003-0352-2, 2003.

Meissner, K. J., McNeil, B. I., Eby, M., and Wiebe, E. C.: The importance of the terrestrial weathering feedback for multi-millennial coral reef habitat recovery, Global Biogeochem. Cy., 26, 1–20, https://doi.org/10.1029/2011GB004098, 2012.

Menge D., Hedin, L., Pacala S.: Nitrogen and Phosphorus Limitation over Long-Term Ecosystem Development in Terrestrial Ecosystems, PLOS ONE 7(8), https://doi.org/10.1371/journal.pone.0042045, 2012.

710   Mengis, N., Partanen, AI., Jalbert, J. et al. 1.5 °C carbon budget dependent on carbon cycle uncertainty and future non-CO2 forcing. Sci Rep 8, 5831. 2018. https://doi.org/10.1038/s41598-018-24241-1

Mengis, N., Keller, D. P., MacDougall, A. H., Eby, M., Wright, N., Meissner, K. J., Oschlies, A., Schmittner, A., MacIsaac, A. J., Matthews, H. D., and Zickfeld, K.: Evaluation of the University of Victoria Earth System Climate Model version 2.10 (UVic ESCM 2.10), Geosci. Model Dev., 13, 4183–4204, https://doi.org/10.5194/gmd-13-4183-2020, 2020.

715 Montenegro, A., Brovkin, V., Eby, M., Archer, D., and Weaver, A. J. Long term fate of anthropogenic carbon, Geophys. Res. Lett., 34, L19707. 2007. doi:10.1029/2007GL030905.

Myhre, G., Stocker, F., Qin, D., Plattner, G, Tignor,M., Allen, S., Boschung, J., Nauels, A., Xia, Y., Bex, V. and Midgley, P.: Anthropogenic and natural radiative forcing. Working Group I Contribution to the Intergovernmental Panel on Climate Change Fifth Assessment Report Climate Change 2013: The Physical Science Basis, Eds., Cambridge University Press. 2013.

720 Nakhavali, M., Mercado, L., Hartley, I., Sitch, S., Cunha, F., di Ponzio, R., Lugli, L., Quesada, C., Andersen, K., Chadburn, S., Wiltshire, A., Clark, D., Ribeiro, G., Siebert, L., Moraes, A., Schmeisk Rosa, J., Assis, R., and Camargo, J. L.: Representation of phosphorus cycle in Joint UK Land Environment Simulator (vn5.5JULES-CNP), Geosci. Model Dev. Discuss. [preprint], https://doi.org/10.5194/gmd-2021-403.

Nzotungicimpaye, Claude-Michel Zickfeld, Kirsten Macdougall, Andrew H Melton, Joe Treat, Claire Eby, Michael Lesack, Lance.
725 WETMETH 1.0: A new wetland methane model for implementation in Earth system models, Geoscientific Model Development, 14, 6215-6240, 2021 10.5194/gmd-14-6215-2021.

Olander, L., and Vitousek, P.: Regulation of soil phosphatase and chitinase activity by N and P availability.Biogeochemistry 49, 175–190, 2000.

Pahlow, M., Chien, C.-T., Arteaga, L. A., and Oschlies, A.: Optimality-based non-Redfield plankton–ecosystem model (OPEM v1.1) in
730 UVic-ESCM 2.9 – Part 1: Implementation and model behaviour, Geosci. Model Dev., 13, 4663–4690, https://doi.org/10.5194/gmd-13-4663-2020, 2020.

Pacanowski, R. C.: MOM 2 Documentation, users guide and reference manual, GFDL Ocean Group Technical Report 3, Geophys, Fluid Dyn. Lab., Princet. Univ. Princeton, NJ, 1995.

Poulter, B., MacBean, N., Hartley, A., Khlystova, I., Arino, O., Betts, R., Bontemps, S., Boettcher, M., Brockmann, C., Defourny, P., Hage-
735 mann, S., Herold, M., Kirches, G., Lamarche, C., Lederer, D., Ottlé, C., Peters, M., and Peylin, P.: Plant functional type classification for earth system models: results from the European Space Agency's Land Cover Climate Change Initiative, Geosci. Model Dev., 8, 2315–2328, https://doi.org/10.5194/gmd-8-2315-2015, 2015.

Reed, S. C., Townsend, A. R., Davidson, E. A., and Cleveland, C.: Stoichiometric patterns in foliar nutrient resorption across multiple scales. New Phytol. 196, 173–180. 2012. doi: 10.1111/j.1469-8137.2012.04249.x

740 Reich, P. B. and Oleksyn, J.: Global patterns of plant leaf N and P in relation to temperature and latitude, Proc. Natl Acad. Sci. 101,11001–11006, doi:10.1073/pnas.0403588101, 2004.

Ryan PR, Dessaux Y, Thomashow LS, Weller DM. Rhizosphere engineering and management for sustainable agriculture. Plant and Soil 321(1–2), 363–383. doi:10.1007/s11104-009-0001-6. 2009.

Schlesinger, W.H.: Biogeochemistry: An Analysis of Global Change. San Diego, USA: Academic Press, 588pp. 1997.

745 Smil, V.: Phosphorus in the environment: natural flows and human interferences, Annual Review of Energy and Environment, 25,53–88, 2000.

Spafford, L. and MacDougall, A. H.: Validation of terrestrial biogeochemistry in CMIP6 Earth system models: a review, Geosci. Model Dev., 14, 5863–5889, https://doi.org/10.5194/gmd-14-5863-2021, 2021.

Shi, M., Fisher, J. B., Brzostek, E. R., Phillips, R. P. (2016). Carbon cost of plant nitrogen acquisition: global carbon cycle impact from an improved plant nitrogen cycle in the Community Land Model. Global change biology, 22(3), 1299-1314.

Thum, T., Caldararu, S., Engel, J., Kern, M., Pallandt, M., Schnur, R., Yu, L., and Zaehle, S.: A new model of the coupled carbon, nitrogen, and phosphorus cycles in the terrestrial biosphere (QUINCY v1.0; revision 1996), Geosci. Model Dev., 12, 4781–4802, https://doi.org/10.5194/gmd-12-4781-2019, 2019.

Tian, H. et al. A comprehensive quantification of global nitrous oxide sources and sinks, Nature, 2020 DOI:10.1038/s41586-020-2780-0

Thornton, P., Lamarque, J., Rosenbloom, N., and Mahowald, N.: Influence of carbon-nitrogen cycle coupling on land model response to CO_2 fertilization and climate variability, Global Biogeochem. Cycles 21, doi:10.1029/2006GB002868, 2007.

Tokarska, K. B., Zickfeld, K., Rogelj, J. Path independence of carbon budgets when meeting a stringent global mean temperature target after an overshoot. Earth's Future, 7, 1283– 1295. 2019. https://doi.org/10.1029/2019EF001312

Wagg C, Bender S, Widmer F, Van der Heijden M. Soil biodiversity and soil community composition determine ecosystem multifunctionality. Proceedings of the National Academy of Sciences 111(14), 5266–5270. doi:10.1073/pnas.1320054111. 2014.

Walker, T. and Syers, J.: The fate of phosphorus during pedogenesis, Geoderma 15, 1-19, doi.org/10.1016/0016-7061(76)90066-5, 1976.

Walker, A., Beckerman, A., Gu, L., Kattge, J., Cernusak, L., Domingues, T., Scales, J., Wohlfahrt, G., Wullschleger, S. and Woodward, I.: The relationship of leaf photosynthetic traits - Vcmax and Jmax - to leaf nitrogen, leaf phosphorus, and specific leaf area: A meta-analysis and modeling study. Ecology and Evolution. 4. 2014.

Wania, R., Meissner, K., Eby, M., Arora, V., Ross, I., and Weaver, A.: Carbon-nitrogen feedbacks in the UVic ESCM, Geosci. Model Dev., 5, 1137–1160, https://doi.org/10.5194/gmd-5-1137-2012, 2012.

Wang, Y., Houlton, B., Field, C.: A model of biogeochemical cycles of carbon, nitrogen, and phosphorus including symbiotic nitrogen fixation and phosphatase production. Global Biogeochemical Cycles 21, 2007.

Wang, Y., Law, R., Pak, B.: A global model of carbon,nitrogen and phosphorus cycles for the terrestrial biosphere, Bio-geosciences 7, 2261–2282,doi:10.5194/bg-7-2261-2010, 2010.

Wang, Y., Ciais, P., Goll, D., Huang, Y., Luo, Y., Wang, Y.-P., Bloom, A. A., Broquet, G., Hartmann, J., Peng, S., Penuelas, J., Piao, S., Sardans, J., Stocker, B. D., Wang, R., Zaehle, S., and Zechmeister-Boltenstern, S.: GOLUM-CNP v1.0: a data-driven modeling of carbon, nitrogen and phosphorus cycles in major terrestrial biomes, Geosci. Model Dev., 11, 3903–3928, https://doi.org/10.5194/gmd-11-3903-2018, 2018.

Wang, Z., Tian, H., Yang, J., Shi, H., Pan, S., Yao, Y., et al. (2020). Coupling of phosphorus processes with carbon and nitrogen cycles in the dynamic land ecosystem model: Model structure, parameterization, and evaluation in tropical forests. Journal of Advances in Modeling Earth Systems, 12, e2020MS002123. https://doi.org/10.1029/2020MS002123

Weaver, A. J., Eby, M., Wiebe, E. C., Bitz, C. M., Duffy, P. B., Ewen, T. L., Fanning, A. F., Holland, M. M., MacFadyen, A., Matthews, H. D., Meissner, K. J., Saenko, O., Schmittner, A., Wang, H. X., and Yoshimori, M.: The UVic Earth System Climate Model: Model description, climatology, and applications to past, present and future climates, Atmos. Ocean, 39, 361–428, 2001.

Weber, S. The utility of Earth system Models of Intermediate Complexity (EMICs). Wiley Interdiscip Rev-Climate Change. 2010. 1. 10.1002/wcc.24.

Wieder, W., Cleveland, C., Smith, W. and Todd, K.: Future productivity and carbon storage limited by terrestrial nutrient availability, Nature Geosci 8, 441–444, https://doi.org/10.1038/ngeo2413, 2015.

Van Oijen, Marcel Barcza, Zoltán Confalonieri, Roberto Korhonen, Panu Kroel-Dulay, Gyorgy Lellei-Kovács, Eszter Louarn, Gaëtan Louault, Frédérique Martin, Raphael Moulin, Thibault Movedi, Ermes Picon-Cochard, Catherine Rolinski, Susanne Viovy, Nicolas

Wirth, Stephen Bellocchi, Gianni. (2020). Incorporating Biodiversity into Biogeochemistry Models to Improve Prediction of Ecosystem Services in Temperate Grasslands: Review and Roadmap. Agronomy. 10. 10.3390/agronomy10020259.

Vitousek, P.M., Porder, S., Houlton, B.Z. and Chadwick, O.A.: Terrestrial phosphorus limitation: mechanisms, implications, and nitrogen–phosphorus interactions, Ecological Applications, 20: 5-15, 2010. https://doi.org/10.1890/08-0127.1

Xu-Ri and Prentice, I. C.: Terrestrial nitrogen cycle simulation with a dynamic global vegetation model, Glob. Change Biol., 14, 1745–1764, 2008.

Yang, X., Post, W.,Thornton, P., Jain, A.: The distribution of soil phosphorus for global biogeochemical modeling,Biogeosciences 10, 2525–2537, https://doi.org/10.5194/bg-10-2525-2013, 2013.

Yang, X. J., Wittig, V., Jain, A. K., and Post, W.: Integration of nitrogen cycle dynamics into the Integrated Science Assessment Model for the study of terrestrial ecosystem responses to global change, Global Biogeochem. Cy., 23, 121–149, 2009.

Yang G, Wagg C, Veresoglou SD, Hempel S, Rillig MC (2018) How soil biota drive ecosystem stability. Trends in Plant Science 23(12), 1057–1067. doi:10.1016/j.tplants.2018.09.007

Yang, X., Ricciuto, D. M., Thornton, P. E., Shi, X., Xu, M., Hoffman, F., Norby, R. J. The effects of phosphorus cycle dynamics on carbon sources and sinks in the Amazon region: a modeling study using ELM v1. Journal of Geophysical Research: Biogeosciences, 124, 3686–3698. 2019. https://doi.org/10.1029/2019JG005082.

Zaehle, S., Friend, A. D., Friedlingstein, P., Dentener, F., Peylin, P., and Schulz, M.: Carbon and nitrogen cycle dynamics in the OCN land surface model: 2. Role of the nitrogen cycle in the historical terrestrial carbon balance, Global Biogeochem. Cy., 24, doi:10.1029/2009GB003522, 2010.

Zaehle, S., Medlyn, B. E., de Kauwe, M. G., Walker, A. P., Dietze, M. C., Hickler, T., Luo, Y., Wang, Y. P., El-Masri, B., Thornton, P., Jain, A., Wang, S., Warlind, D., Weng, E., Parton, W., Iversen, C. M., Gallet-Budynek, A., Mccarthy, H., Finzi,A.,Hanson, P., Colin I., Oren R. and Norby, R.: Evaluation of 11 terrestrial carbon-nitrogen cycle models against observations from two temperate Free-Air CO_2 Enrichment studies, New Phytologist, 202(3), 803–822, https://doi.org/10.1111/nph.12697, 2014.

Zickfeld, K., Eby, M., Matthews, H. D., and Weaver, A. J.: Setting cumulative emissions targets to reduce the risk of dangerous climate change, P. Natl. Acad. Sci. USA, 106, 16129–16134, https://doi.org/10.1073/pnas.0805800106, 2009.

Ziehn, T., Chamberlain, M., Law R., Lenton, A., Bodman, R., Dix, M., Stevens L., Wang, Y., Srbinovsky, J. The Australian Earth System Model: ACCESS-ESM1.5. Journal of Southern Hemisphere Earth Systems Science 70, 193-214. 2020.